The Topology Design Principles that Determine the Spatiotemporal Dynamics of G-protein Cascades.

Mikhail A. Tsyganov[1,2], Walter Kolch[2] and Boris N. Kholodenko[2,3*]

[1]Institute of Theoretical and Experimental Biophysics, Pushchino, Moscow Region, Russia
[2]Systems Biology Ireland, University College Dublin, Belfield, Dublin 4, Ireland,
[3]Thomas Jefferson University, Department of Pathology, Anatomy, and Cell Biology, Philadelphia, PA 19107, USA

Running title: Spatiotemporal Dynamics of G-protein cascades

The sentence highlighting the novelty of the work.
This work elaborates the first classification of 128 possible topologies for two-tier GTPase cascades in terms of their spatiotemporal dynamics.

*To whom correspondence should be addressed.
E-mail: boris.kholodenko@ucd.ie

Abstract.

Small monomeric G-proteins control cellular behavior, cycling between inactive GDP-bound and active GTP-bound states. Activating and deactivating transitions are regulated by guanine nucleotide exchange factors (GEFs) and GTPase activating proteins (GAPs), respectively. G-proteins can control different GEF and GAP activities, thereby creating GTPase signaling cascades. Here, we characterize all 128 different wiring topologies of two-layer cascades, which include feedforward/feedback interactions and an auto-regulatory loop. Exclusion of "mirror" designs leaves 64 topologies, which are classified into eight groups. We demonstrate that eight different cascades in each group generate the same number of steady states and similar spatiotemporal dynamics. Two groups (featuring 16 topologies) can generate three distinct dynamics: (*i*) bistable switches, (*ii*) excitable behavior, and (*iii*) sustained oscillations, giving rise to propagating waves of G-protein activation switches and pulses. Four other groups can produce switch-like, bistable behaviors and trigger waves. The remaining two groups have a single steady state. This first, complete classification of all possible interaction circuitries systematically links topological design to the spatiotemporal dynamics of G-protein cascades, predicting and explaining experimentally observed behavior.

Introduction

Small monomeric G-proteins (GTPases) comprise a superfamily of more than a hundred proteins with GTPase activities [1]. Small GTPases are found in all eukaryotes, from yeast to humans, where they regulate intracellular signaling, cytoskeletal rearrangements and vesicle transport. A GTPase cycles between an inactive GDP-bound form and an active GTP-bound form. Active GTPases stimulate downstream effector kinases and other proteins, thereby turning on key cellular processes, such as migration or mitogenesis [2, 3]. The cycling of GTPases between inactive and active states is catalyzed by guanine nucleotide exchange factors (GEFs), which facilitate GDP/GTP exchange and the transition to the active, GTP-bound state, and GTPase activating proteins (GAPs), which stimulate GTP hydrolysis and the transition to the inactive, GDP-bound state. Crosstalk between functional cycles of different GTPases generates signaling cascades where each GTPase may positively or negatively control GEFs or GAPs at its level and other cascade levels [4-6]. Experimentally observed examples of such cascades include a cascade of interacting Rab GTPases that control the conversion of early endosomes into late endosomes [7] and cascades of the Rho family GTPases that regulate cytoskeleton dynamics and cell motility [8, 9].

The three members of the Rho GTPase family, Cdc42, Rac1 and RhoA, have been most extensively studied owing to their pivotal role in cellular responses to growth factors, cytokines and other hormones. Experimental data show that Cdc42, Rac1 and RhoA mutually regulate each other activities. It was suggested that Cdc42 activates Rac1, while Rac1 can both inhibit and activate RhoA, and RhoA can inhibit Rac1 [10-12]. Importantly, these positive and negative interactions in GTPase cascades can bring about dynamic instabilities in time and space [13]. In fact, both computational models and experimental data show that some GTPase cascades exhibit intricate spatiotemporal dynamics, including bistable switches, oscillations, and symmetry-breaking driven by the Turing-type instabilities [7, 14-18]. Despite such intriguing experimental observations, the general relationship between the molecular interaction topologies of GTPase cascades and their observed spatiotemporal dynamic behaviors remain poorly characterized [19]. For instance, it is unclear if differently wired GTPase cascades can exhibit similar spatiotemporal dynamics, and what particular features of diverse molecular designs can make the dynamic behavior of cascades to be similar or different from each other. Furthermore, complex dynamic behavior was predicted to occur for the cooperative, Hill kinetics [18], and it remains unclear what spatiotemporal dynamics would be observed if reactions follow the standard, Michaelis-Menten kinetics.

Temporal and spatial controls cooperate to coordinate pivotal biological processes and often exploit pre-existing heterogeneity within a cell [12, 20]. This spatial heterogeneity facilitates the generation of positional information [21, 22]. Even if a GTPase cascade displays only a single, stable steady state, the spatial segregation of GEFs and opposing GAPs on different cellular structures can result in complex spatial patterns of GTPase activities [6, 23-25]. Such complex activity profiles were observed for a chromosome-

dependent RanGTPase-importin cascade [26, 27]. In addition to the stationary positional information generated by monostable cascades, intricate dynamic patterns of information transfer can arise in GTPase cascades with multi-stable and oscillatory kinetics. For instance, in bistable cascades global switches of GTPase activation can be brought about by spatially confined signals that locally perturb GEF and/or GAP activities [28-30]. Similar traveling waves have been studied in physics and biology [31-33]. However, the implications of the spatial heterogeneity coupled with different types of cascade dynamics (such as excitable and oscillatory behaviors) for the propagation of GTPase activation in the cellular space remain largely unexplored.

The present paper explores the complete set of regulatory circuitry designs for cascades of two GTPases. It analyzes the spatiotemporal dynamics of a cascade where an active, GTP-bound GTPase at one layer activates or inhibits a GEF or GAP at the other layer and, in addition, can activate or inhibit its own GEF or GAP, thereby generating an auto-activation or auto-inhibition loop. Such auto-regulatory loops have been experimentally observed for the small GTPases Ras and Cdc42, which bind and activate their own GEFs [34, 35]. Our analysis shows that the overall set of possible molecular topologies of G-protein cascades with a single auto-regulatory loop can be divided into 8 groups with 8 members each (due to the mirror symmetry, only 64 out of possible 128 circuitries have to be considered, see below). We further demonstrate that 8 different cascade circuitries in each group can display the same number of steady states and similar dynamics in time and space, and, thus, can be termed "quasi-equivalent". Two of the eight groups can exhibit abrupt, bistable switches, excitable behavior, and sustained oscillations. The corresponding cascade topologies are hallmarked by an auto-activation loop and negative feedback from one GTPase to the other (specific for a group). In space, these topologies give rise to nonlinear traveling waves, which propagate pulses or global switches of GTPase (de)activation. GTPase cascades comprising four other groups show switch-like, bistable behaviors and trigger spatial waves, whereas cascades in the remaining two groups have a single stable steady state. We further show how the spatial heterogeneity, including gradients of the GEF or GAP concentration, brings about intricate dynamic patterns of propagation of GTPase activity in cellular space. Thus, our results provide the first classification of all 128 possible interaction circuitries for two-tier GTPase cascades in terms of their dynamics in time and space.

Results

Molecular interaction topologies. We first characterize the overall set of regulatory designs for a two-layer GTPase cascade. At each cascade layer, a GEF catalyzes the transition of an inactive GTPase form (G) into an active form (GP), while a GAP catalyzes the reverse transition (GP into G). An active GTPase can interact with its own GEF or GAP, thereby generating an auto-regulatory loop, and also with GEF and GAP for the other GTPase [7]. We assume that only one of two GTPases, for instance, G_1P, auto-regulates itself. There are four possible auto-regulatory circuitries, two of which correspond to G_1P-

mediated activation or inhibition of its GEF, and the other two topologies correspond to G_1P-mediated activation or inhibition of its GAP (Fig. 1a). Taking into consideration that G_1P and G_2P also influence GEF or GAP at the opposite layer and each interaction can be inhibitory or activating, we find that there are in total $4^3 = 64$ different circuit architectures for a two layer GTPase cascade.

Fig. 1b presents all 64 molecular topologies using only eight "influence" diagrams where G_1P and G_2P are shown by bold dots. Every stimulatory influence (a red line with an arrow head) corresponds to either GEF activation or GAP inhibition and every inhibitory influence (a blue line with a blunt end) corresponds to GEF inhibition or GAP activation. Each influence diagram generates a group of eight distinct molecular wiring designs (Fig. 2). These different wiring circuitries are similar in terms of inhibitory and stimulatory influences of GTPases on themselves and each other, but they are different in terms of molecular interactions affecting GEFs or GAPs. Note that there are 64 mirror symmetry circuits, which involve auto-activation and auto-inhibition loops mediated by G_2P (rather than G_1P). Since each mirror circuit is obtained by simple renumbering of cascade layers, we consider the spatiotemporal dynamics of only 64 interaction topologies presented in Fig. 1b, and our results completely characterize all 128 potential interaction designs.

Several questions arise with respect to influence diagrams presented in Fig. 1b. Will the eight different wiring designs within each group exhibit similar or diverse dynamic behavior in time and space? What are the differences in the spatiotemporal G-protein dynamics between different groups of designs? And how do distinct temporal dynamics affect the propagation of activating or inhibitory signals within a cell? Answers to these questions can be obtained by mathematical exploration of the spatiotemporal behavior of the 64 GTPase cascades. To examine the dynamics of each cascade in time and space, we will next analyze differential equations that describe the reaction kinetics and diffusion of GTPases.

Dynamics of spatially homogenous cascades.

A generalized kinetic description of 64 possible regulatory topologies. For a well-mixed compartment, the temporal dynamics of GTPase cascades are governed by ordinary differential equations. For simplicity, we assume that the rates of GEF and GAP-catalyzed reactions can be described by the Michaelis-Menten expressions where the regulatory influences of GTPases on GEFs and GAPs correspond to pure non-competitive mechanisms of enzyme inhibition or activation. This allows us to present any reaction rate (v_j) as the product of the Michaelis-Menten rate (in the absence of regulatory interactions) and modifying, dimensionless multipliers, $\alpha_{ij}(G_iP)$, which specify the auto-regulatory, feedforward or feedback influence of G_iP on the rate v_j (Eqs. 1 and 2 in Methods). Each multiplier $\alpha_{ij}(G_iP)$ is described by a Michaelis-Menten type function of the corresponding active GTPase fraction [36], where the maximal degree of activation or inhibition is determined by the coefficient a_{ij}. An $a_{ij} > 1$ indicates activation; $a_{ij} < 1$

inhibition; and $a_{ij} = 1$ indicates the absence of regulatory interactions, in which case the modifying multiplier $\alpha_{ij}(G_iP)$ equals 1 (Eqs. 2 in Methods). On the time scale considered, the total concentrations of inactive and active GTPase forms are conserved: $G_1 + G_1P = G_1^{tot}$ and $G_2 + G_2P = G_2^{tot}$. Consequently, active GTPase fractions, $g_1p = G_1P / G_1^{tot}$ and $g_2p = G_2P / G_2^{tot}$, can be described as dimensionless, independent variables (Eqs. 3 and 4 in Methods). An advantage of this description of GTPase cascade topologies and dynamics is that each of the 64 different wiring designs is uniquely specified by the dimensionless multipliers α_{ij}, which define activating or inhibiting loops when these multiplies are greater or less than 1. For instance, each of the eight different designs comprising group I corresponds to the following constraints on modifying multipliers, $\alpha_{11} > 1$ *or* $\alpha_{12} < 1$, $\alpha_{21} < 1$ *or* $\alpha_{22} > 1$, and $\alpha_{13} > 1$ *or* $\alpha_{14} < 1$ (Fig. 2). Equations given in Methods (Table 1) conveniently present eight different kinetic designs for any group I - VIII shown in Fig. 1b (see also Supplementary Information 1 (SI 1) that shows how the values of the dimensionless multipliers α_{ij} specify each design group).

Analysis of steady-state behaviors of GTPase cascades.

Stationary behaviors are similar for cascades within each group, but can differ between groups. We first explore if different regulatory circuitries of GTPases cascades can display similar steady-state behaviors, including (*i*) the same number and (*ii*) identical local stability properties of the steady states. It is convenient to analyze cascade behaviors on the plane of active GTPase fractions (g_1p, g_2p) that is referred to as a phase plane. By considering steady-state conditions separately for g_1p ($dg_1p/dt = 0$) and g_2p ($dg_2p/dt = 0$), we arrive at two different curves known as nullclines (illustrated in Fig. 3), which relate the GTPase activities when one of GTPases is in steady state. Importantly, for each GTPase cascade the points of intersections of these two nullclines present all plausible steady states.

SI 2 shows analytically that under the proper conditions for the kinetic parameters of regulatory loops, the nullclines and, therefore, all steady states become identical for eight cascade designs within each group, whereas these steady states are different for different groups I - VIII (schematically shown in Fig. 1b). The corresponding parameter relationships that guarantee the identity of the nullclines and steady states for all cascades within each group are given in Table 1 in Methods. In addition, for the equivalence of steady-state behaviors of the eight different cascades in each group, the stability properties and local bifurcations of the steady states should be the same. SI 3 contains a mathematical proof that if certain relationships between kinetic parameters are fulfilled, the equations describing any of the eight different cascades within each group have identical eigenvalues, which determine the cascade stability properties. Consequently, these eight cascades display similar steady-state behaviors, although these behaviors differ between groups I - VIII. Importantly, the reaction rates remain different for distinctly wired cascade circuitries within a group.

Therefore, the temporal dynamics are not identical, although these dynamics can be similar for cascades within each group, as we will see below. Consequently, we term quasi-equivalent the eight kinetic circuitries that constitute each group (I- VIII). Next, we will explore the stationary behaviors for each group I - VIII.

Bistable behaviors. A dynamic system that switches between two distinct, stable steady states and cannot rest in an intermediate, unstable state is called bistable. Bistable behaviors of signalling cascades are often brought about by explicit or implicit positive feedback motifs [37-39]. For a single GTPase cycle, bistability can arise from activation of a GEF by its product, which is an active GTPase (product activation, positive feedback), or inhibition of a GAP by its substrate, an active GTPase (substrate inhibition, negative feedforward loop) [13, 40]. Accordingly, one may conjecture that molecular topologies within groups I – IV, where G_1P stimulates itself by activating its own GEF or inhibiting its GAP, may display bistability. Topologies in groups V and VI where two active GTPases, G_1P and G_2P, activate or inhibit each other resemble positive or double negative interaction loops, which have also been shown to result in bistability [18, 41]. However, since a proper degree of cooperativity is required for bistability [18, 37], it remains unclear, if the Michaelis-Menten kinetics of interaction loops can bring about bistable behaviors of signaling cascades in groups V and VI.

The occurrence of bistability can readily be perceived by plotting two nullclines on the plane g_1p, g_2p, since all steady states correspond to the points where these curves intersect. We next show that for cascades in groups I, II, III and IV, which are hallmarked by the auto-activation loop from G_1P (Fig. 1b), the g_1p nullcline, $dg_1p/dt = 0$, can display an "N" shape (which is characterized by two extrema: maximum and then minimum), or "N-mirror" shape (minimum followed by a maximum), left panels, Fig. 3. At the same time, the g_2p nullcline, $dg_2p/dt = 0$, is a monotone curve (as demonstrated analytically in SI 4). As a result, depending on choice of parameters there can be one or three nullcline intersection points and, consequently, one or three steady states of a cascade (left panels, Fig. 3). Three intersection points correspond to bistability, when there are two stable states (indicated as S_1 and S_2) and an intermediate unstable steady state (U). The right panels in Fig. 3 show how active, stationary GTPase fractions (g_1p and g_2p) vary with the change in the "input", which is taken as the maximal GEF_1 activity for illustrative purposes (parameter r_1 in Eq. 3). We can see that g_1p and g_2p behave as toggle switches, responding to gradually increasing or decreasing input stimuli.

Bistable systems always display hysteresis, meaning that the stimulus must exceed a threshold to switch the system to another steady state, at which it may remain even when the stimulus decreases. For instance, for groups I and III a stimulus that causes an increase in GEF_1 activity leads to an abrupt switching on of both GTPase activities once this stimulus exceeds the threshold P_1 (called turning point, Fig. 3). The switch amplitude is much larger for g_1p (that undergoes a complete "Off" to "On" switch) than for g_2p,

whose active fraction is already substantial at sub-threshold GEF_1 activity. To return to the initial "Off" state, the stimulus should decrease below the critical value that corresponds to turning point P_2, Fig. 3. Thus, GTPase activity can be high or low under the exact same condition depending on whether the stimulus was higher or lower than the threshold (the stimulation history). For groups II and IV, an increase in GEF_1 activity leads to an "On" switch of GTPase activity at the upper cascade level (g_1p), but it abruptly decreases GTPase activity at the lower level (g_2p). The difference between coherent switches of both GTPases in cascades comprising groups I and III and opposite switches of GTPases in groups II and IV can be explained by different topology features of GTPase interactions in the cascades comprising these groups. In groups I and III, G_1P activates G_2P, whereas in groups II and IV, G_1P inhibits G_2P. Likewise, bistable switches in GTPase activity may be observed for gradual changes in GAP concentrations rather than GEF concentrations (Supplementary Fig. S1).

For cascade topologies in groups V - VIII, each hallmarked by an auto-inhibition loop (Fig. 1b), we demonstrate analytically (SI 4) that the g_1p-nullclines are monotone and, thus, cannot display N (or N-mirror) shapes, whereas the g_2p-nullclines are monotone for all possible topologies and parameter values in all groups I - VIII. Importantly, both nullclines increase monotonically for cascades in group V, and decrease monotonically for cascades in group VI. In this case where slopes have identical sign, the nullclines may have up to three intersection points, which is observed, in fact, for cascades in groups V and VI (Fig. 3). At both upper and lower tiers of cascades comprising group V, an increase in GEF_1 activity results in a coherent GTPase switch from an "Off" state to an "On" state, whereas these GTPases exhibit opposite switches for cascades included in group VI (g_1p undergoes an "On" switch, while g_2p undergoes an "Off" switch). For cascades in groups VII and VIII, one nullcline is a monotone increasing function, whereas the other is a monotone decreasing function, thus these nullclines cannot intersect more than once (typical nullclines of VII and VIII groups are shown in Fig. S2). We conclude that 48 different cascades from molecular topology groups I - VI can display bistable behavior, whereas 16 cascades in groups VII and VIII are monostable. Note that for all eight different cascade designs within a group, the hysteresis curves are identical, provided that the relationships between kinetic parameters enabling the identity of steady states of different cascades are satisfied (Table 1, Methods). Therefore, the hysteresis curves are shown only for topology design 1 for groups I - VI (Fig. 3).

Oscillatory dynamics and excitable, overshooting transitions of GTPases.

Sustained oscillatory behavior. Oscillations of GTPase activities have been both observed experimentally and studied theoretically [14, 42]. A mathematical prerequisite for sustained oscillations in a two-layer GTPase cascade is illustrated in Fig. S3a, where the N (or N-mirror)-shaped nullcline and the monotone nullcline intersect at a single point corresponding to an unstable steady state. Consequently, the cascade cannot reside at the steady state, but oscillates in a self-perpetuating manner with constant

amplitude and period (Fig. 4a-d). Such oscillations occur because a part of the cascade (the upper cycle) is potentially bistable, while both GTPase cycles oppositely influence each other (one GTPase activates the other, which in turn inhibits the former). This creates a negative feedback loop that periodically forces the system to jump between two distinct states (which otherwise would be observed in the bistable regime), generating oscillations [13, 41, 43]. Such positive-and-negative feedback loop oscillations, which are often referred to as relaxation oscillations, operate in a pulsatory manner and generally do not have sinusoidal shapes (Fig. 4a-d) [44-46].

While 48 differentially wired cascades of two GTPases can exhibit switch-like bistable behaviors (groups I - VI), only 16 cascade topologies comprising groups I and II display sustained oscillations (since potential bistability must be coupled with a negative feedback loop). When analyzing bistability, we have seen that the hysteresis curves that display stationary behaviors coincide for all eight distinct topology designs within each group that exhibits bistability (groups I - VI, Fig.3), provided that the parameters of regulatory interactions are properly constrained (Table II). Unlike hysteresis curves, oscillatory and excitable dynamics differ for different wiring designs within a group (compare different periods and shapes of oscillations for designs 1 and 5 (in group I or II) shown in Fig. 4a-d). Importantly, depending on both the molecular topology design and kinetic parameter values the period of oscillations can vary from a few seconds to tens of minutes or an hour, which endows a cell with flexible spatiotemporal ruler for the guiding of pivotal biochemical processes by GTPase activities (see the section on spatially distributed signaling below). Sustained oscillations displayed by all cascades in groups I and II are presented in Fig. S3.

Excitable pulses of GTPase activity. Interestingly, 16 GTPase cascades comprising groups I and II can also exhibit excitable dynamics. These excitable responses resemble the behavior of classic excitable systems, such as action potential in neurons or heart Purkinje fibres. We assume that a GTPase cascade initially resides at a stable, but excitable steady state. Depending on the magnitude of a transient perturbation, responses of GTPase activities will fit into two distinct classes of either low or high amplitude responses (whereas there are no intermediate responses that are simply proportional to the perturbing stimulus). Such excitable behaviors are illustrated in Fig. 4e-h. For sub-threshold perturbations, GTPase activities rapidly return to their basal values (the corresponding time evolution is shown by dashed lines). However, if the perturbation amplitude exceeds a threshold value, a large overshoot response occurs before GTPase activities return to the basal state (solid lines, Fig. 4e-h). The sign and magnitude of overshoot responses (spikes of increasing or declining GTPase activities) depend on the cascade topology and the initial excitable steady state. As illustrated in Fig. S4, excitable responses to a transient perturbation of stationary GTPase activities occur when a cascade has a single, stable steady state, which is an intersection of the monotone and N (or N-mirror)-shaped nullclines in the plane of GTPase activities. If the initial steady state is localized sufficiently close to an unstable steady state corresponding to the oscillatory regime, the

threshold perturbation amplitude can be very small (Fig. S4, panels a,e and c,g). The lack of oscillatory regimes for GTPase cascade topologies comprising groups III - VI, which exhibit bistable switches of GTPase activities, prevents these cascades from displaying such excitable behaviors.

We conclude that perturbations to an excitable cascade can cause essentially none-or-all responses. Thus, an excitable GTPase cascade displays features similar to those of a digital device with a built-in excitability threshold. Pulses of GTPase activities brought about by excitable responses of GTPase cascades can be exploited by the cell to rapidly transfer information in time and space, as we will illustrate in the next section.

Spatial signaling by GTPase cascades.

A living cell does not resemble the well-stirred enzymologist's test tube. Besides the temporal control, the spatial control plays a major and complementary role in specifying the biological functions of GTPase cascades. The intricate temporal dynamics of GTPase cascades, involving bistable, oscillatory and excitable behaviors have immediate ramifications for the propagation of switches, pulses, and other patterns of GTPase (de)activation within a cell. An exploration of the spatiotemporal dynamics involves the analysis of partial differential equations (known as reaction-diffusion equations), which govern the evolution of protein activities in time and space on the scale of a cell. Spherical symmetry simplifies analysis of signaling in three dimensions, as the protein concentrations become functions only of radial distance and time [21]. Neglecting the curvature effects (see, e.g., [29]), we will further consider a simple, one-dimensional geometry with the Cartesian spatial coordinate that is confined by a typical cell size. The corresponding reaction-diffusion equations that describe the spatiotemporal dynamics of each of the 64 cascades (Fig. 1b) are presented in Methods (Eq. 8).

Global switches and local pulses of GTPase activity propagating in space. We will first assume that kinetic parameters do not change with the spatial coordinate, in particular, there are no gradients of constitutive GEF and GAP activities (described by parameters r_i, Eq. 3, Methods) in space. However, both active GTPase fractions can vary in space. Suppose a cascade initially resides in a stable, spatially homogeneous steady state where stationary GTPase activities do not depend on the spatial coordinate. Let GTPase activity be locally perturbed by a transient signal that is confined to a certain area. This spatially localized and transient GTPase (de)activation can relax to the original, spatially homogeneous steady state or propagate within a cell [17, 30]. We next illustrate two different modes of signal propagation in space and time: global switches and pulse-like traveling waves of GTPase (de)activation occurring in bistable and excitable GTPase cascades, respectively.

Abrupt switches of protein activity arising in bistable systems have been implicated in the mechanisms of spatial signal propagation by bistable protein-modification cascades [28, 29]. Here we consider a bistable GTPase cascade, which can be any of 48 different cascades comprising groups I - IV that exhibit

bistable switches. Let the GTPase of interest initially reside in the low activity, basal state that is maintained over the entire cellular space ("Off" state). Suppose that following local, transient stimulation (perturbation), this GTPase activity has increased and exceeded a threshold of switching to a high activity, stationary state ("On" state) within a confined area of space (see the spatial profile of the active GTPase fraction g_1p at time zero in Fig. 5a). Active GTPase molecules can then diffuse and activate other molecules of the same GTPase through autoactivatory interactions (topology designs in groups I - IV) and/or through positive or dual negative interactions between GTPases (groups III - VI). This can flip GTPase activity into the "On" state within the adjacent space area, thereby generating a self-perpetuating, travelling wave that switches a GTPase "On" globally in space following local activation (see spatial profiles at subsequent time points in Fig. 5a). A mirror scenario corresponds to the initial "On" state of the GTPase of interest and the local inhibitory signal that can switch the activity to the "Off" state in space (Fig. 5b). Since traveling waves propagate with a constant speed, the time of the signal transfer increases linearly with the cell size, whereas the time of signal propagation by diffusion is proportional to the square of the cell size. This is a reason why travelling waves can effectively transfer protein modification signals [47].

In addition to global switches (trigger waves) that can propagate in bistable GTPase cascades, excitable properties of the cascades comprising groups I and II can bring about travelling, excitable waves of GTPase (de)activation pulses (Fig. 5c,d), as well as other self-perpetuating spatial patterns in two and three spatial dimensions. A key feature of propagating GTPase activation waves is that a particular molecule of an active GTPase would not have to diffuse all the way from the place of activation. Rather, the spread of activation in a cell emerges as a result of a combination of diffusion and rapid excitation at the wave front following the arrival of active GTPase molecules by diffusion (Fig. 5c). A mirror scenario corresponds to propagating pulses of GTPase deactivation (Fig. 5d).

Heterogeneity of the distribution of GAP and/or GEF activities. Signaling pathways are spatially organized in living cells. Often, an activating enzyme and opposing deactivating enzyme are localized to distinct cellular structures [26, 47]. For instance, activating signals can occur on the plasma membrane or intracellular membranes where receptors and effector-enzymes reside, while deactivating processes can be spread in the cytoplasm. For a protein activated by a membrane-bound kinase and deactivated by a cytosolic phosphatase, a precipitous protein activity gradient was theoretically predicted (with high activity close to the membrane and low activity in the cell interior) [21]. Subsequently, fluorescence resonance energy transfer-based biosensors enabled discoveries of intracellular gradients of the active form of the small GTPase Ran [23, 26], as well as other signaling proteins [48-50]. We next show how the spatial gradients of active concentrations of GAP and/or GEF can influence spatial patterns of activities in GTPase cascades.

For illustrative purposes, we assume that there is a spatial gradient of GAP_2 constitutive activity, which is maximal at the membrane and gradually decreases toward the cell interior. Such a gradient may

arise if GAP_2 is phosphorylated by a membrane kinase (resulting in an increased GAP_2 activity) and dephosphorylated by a cytoplasmic phosphatase. If the kinetics of dephosphorylation is far from saturation, the phosphorylated GAP_2 form will decay almost exponentially, resulting in a significant decrease in GAP_2 activity with the distance from the membrane (Eq. 10, Methods) [21]. For a GTPase cascade that exhibits distinct dynamic behaviors at different kinetic parameter values, this change in the GAP_2 constitutive activity can result in dramatic changes of the temporal cascade responses. For instance, for a cascade in groups I or II, a decrease in GAP_2 activity can result in a switch from the oscillatory behavior to excitable behavior, described mathematically in terms of Hopf bifurcations (cf. Figs. 4a-d and 4e-h where a similar transformation of the cascade dynamics is brought about by a variation of GEF_2 activity only). Let sustained oscillations of the active GTPase fractions be occurring within a local area close to the plasma membrane (Fig. 6a). Suppose that at a distance from the membrane where the GAP_2 constitutive activity has dropped, the cascade switches to excitable dynamics. Accordingly, while the oscillating active GTPase fraction near the cell membrane approaches the maximum, diffusion of active GTPase molecules coupled with the excitable properties of the cascade farther into the cell can result in the propagation of the pulse-like wave of the active GTPase conformation (Fig. 6b, c). Whereas Fig. 6 shows the formation and propagation of GTPase activity pulses happening within a few seconds, depending on the molecular topology design and kinetic parameters, the time scale of GTPase pulse-like waves can vary from seconds to tens of minutes, which accounts for the reported data [12, 51]. Interestingly, while the cell cytoplasm resembles an excitable media, at sufficiently low oscillation frequency, all GTPase activity maxima will propagate through the cell. However, when the frequency increases, the time period between two consecutive oscillation maxima will become smaller than the recovery time of the excitable media, and some pulses will fade away rather than propagate (see Fig. S6). For neurons, heart Purkinje fibres and chemical media, this is known as the refractory period, when the excitable media does not respond to a stimulus [52].

Discussion

Specific cellular behaviors, such as cytoskeletal reorganization, depend on the precise control of the spatiotemporal dynamics of protein activities [20, 53]. The grand challenge is to reveal how cells integrate the temporal and spatial information generated by GTPase cascades to determine specific biological functions [12]. Yet, for multiple interacting GTPases their mutual regulation remains largely unknown. For instance, although it is established that interactions between Cdc42, Rac1 and RhoA coordinate cytoskeletal dynamics with precision of seconds and submicrometers, the reports that examine the regulation of these GTPases are somewhat controversial, suggesting that Rac1 can both inhibit and/or activate RhoA [4, 5, 10, 11, 54-56]. Partly, this controversy is due to the large differences in the expression levels of multiple GEFs and GAPs in different cells and tissues [11]. Moreover, wiring circuitries of GTPase and other protein cascades can also

depend on the cell context, including external cues, and these circuitries can change dynamically depending on activation of specific receptors stimulated by different ligands [20, 57, 58]. This warrants theoretical analyses, which explore molecular designs and relate the interaction topologies to potential dynamic behaviors [13, 59, 60].

Here, we develop the first systematic classification of 128 possible molecular topologies for two-layer GTPase cascades (with a single auto-activation or auto-inhibition loop) in terms of their spatiotemporal dynamics. Since each topology design has a mirror design that is described by renumbering the cascade tiers (GTPases), it was sufficient to analyse only 64 cascade designs. Our analysis shows that these designs can be classified into 8 groups with 8 members which can have identical steady states, as we demonstrate analytically. We also show that the dynamic stability properties of the steady states are identical for 8 cascades within each group, provided that certain relationships between kinetic parameters of regulatory loops are satisfied. As a result, many features of the temporal behavior are the same within a group. Thus, although the manifestation of particular dynamics depends on the kinetic parameter values, the types of plausible behaviors (such as monostable or bistable behavior, excitable and oscillatory dynamics) are primarily controlled by the molecular topology of a cascade.

Our findings support an emerging concept that the dynamic interaction topology of molecular networks controls their physiological or pathological responses. An interesting corollary is the (quasi)equivalence of alternative regulatory mechanisms: under the proper conditions, a GAP activation loop and a GEF inhibition loop can bring about similar spatiotemporal dynamics of GTPase cascades. Mutual inhibition of GTPases for 16 cascade topologies comprising groups IV and VI can lead to abrupt GTPase activity switches and bistability, and thus bistability can be can expected for mutually inhibiting Rac and Rho GTPases [12]. In general, multiple wiring circuitries can display bistable and hysteretic behaviors, as manifested by 48 distinct cascade designs of groups I - VI (Fig. 3). The analysis of 16 molecular topologies comprising groups I and II suggests, that if one GTPase activates the other GTPase, which in turn inhibits the first, and one of these GTPases is self-activating, sustained oscillations and excitable cascade responses can emerge (in addition to bistability). Fig 7 summarizes the distinctive spatiotemporal dynamics for all possible molecular topologies that are classified into eight design groups. The quasi-steady state relationships (known as nullclines) that control the types of the temporal behavior for GTPase activities are shown for the corresponding design groups together with the snapshots of the spatial GTPase activation profiles. For excitable and bistable regimes, these spatial profiles illustrate the propagating activity pulses and global trigger waves, respectively (Fig. 7).

The classification of the dynamics of two-tier motifs may help us understand the spatiotemporal dynamics of GTPase cascades with more than two tiers. As an example we consider a three-tier cascade where GTPases at the first (G_1P) and second (G_2P) layers activate each other, G_2P activates GTPase at the 3rd layer (G_3P), while G_3P inhibits G_2P, Fig. 8a [6]. We notice that if mutual activation of G_1P and G_2P can be

presented as an auto-activation loop for G_2P, the opposing influences of G_2P to G_3P on each other allows us to relate this three-tier cascade wiring with a two-tier cascade design of group I. As a result, we can expect bistable, oscillatory and excitable dynamics, which indeed can be observed (Fig. 8 b, c, d). Obviously, the dynamics of cascades with three or more layers cannot be predicted solely by considering two-tier cascade motifs, but the classification of the spatiotemporal dynamics of these motifs helps us generate hypotheses to be tested computationally and experimentally. The general formalism suggested here is a coarse-grained approximation that greatly facilitates analytical and numerical exploration of the spatiotemporal dynamics of multi-component cellular GTPase cascades and networks. Interestingly, Cdc42 activates its own GEF (p220/DOCK11) [35] and can activate Rac, which in turn activates Rho, while Rho can inhibit Rac and Cdc42 [5, 61]. A combination of auto-activation and opposing influence motifs (groups I and II) suggest intricate dynamics, and, in fact, bistability and oscillations for this interaction topology were predicted theoretically [14, 15].

Complex dynamic behaviors of kinase cascades (e.g., MAPK cascades), such as oscillations, are suggested to have an important physiological role in the control of gene expression on intermediate and long time scales [62-64], but what is the regulatory function of the intricate dynamics of GTPase cascades? Our results suggest that these dynamics enable the precise control of the localization and spatial propagation of active GTPase states that regulate cytoskeletal dynamics and cell motility. Diverse analogue signals can be converted into discrete, digital outputs of bistable and excitable GTPase cascades and/or encoded into the oscillation frequency. Cells are immersed in an ocean of external cues, and some of these signals are spatially heterogeneous, such as chemokine and growth factor gradients or localized signals from neighbouring cells. As a result, the GTPase cascade outputs can be heterogeneous in the cellular space, contributing to the proper regulation of the position-dependent functions, such as the generation of cellular protrusions. These properties enabling versatile yet precise spatiotemporal regulation may account for the widespread occurrence of GTPase cascades in biology.

Materials and Methods

Kinetic equations that describe the 64 possible regulatory topologies.

We consider the time scale, on which the total concentration of inactive and active GTPase forms is conserved, $G_1 + G_1P = G_1^{tot}$, $G_2 + G_2P = G_2^{tot}$. Choosing active GTPase concentrations, G_1P and G_2P, as independent variables, assuming a Michaelis-Menten type of kinetic description for the enzyme rates, and denoting the rates of activation and deactivation reactions by v_1 and v_2 for G_1P and v_3 and v_4 for G_2P (Fig. 1a), the temporal dynamics of each of the 64 cascades are governed by the following ordinary differential equation (ODE) system,

$$\begin{aligned} \frac{dG_1P}{dt} &= v_1 - v_2 \\ \frac{dG_2P}{dt} &= v_3 - v_4 \end{aligned}, \qquad \begin{aligned} v_1 &= \alpha_{11}\alpha_{21}w_1, \quad w_1 = V_1\frac{G_1/K_1}{1+G_1/K_1} \\ v_2 &= \alpha_{12}\alpha_{22}w_2, \quad w_2 = V_2\frac{G_1P/K_2}{1+G_1P/K_2} \\ v_3 &= \alpha_{13}w_3, \quad w_3 = V_3\frac{G_2/K_3}{1+G_2/K_3} \\ v_4 &= \alpha_{14}w_4, \quad w_4 = V_4\frac{G_2P/K_4}{1+G_2P/K_4} \end{aligned} \qquad (1)$$

The rates v_i in Eqn. 1 are described as the products of Michaelis-Menten type expressions w_i (in the absence of positive or negative regulations) and dimensionless, modifying multipliers α_{ij} where indices i and j indicate the GTPase (G_iP) and the reaction rate (v_j) that is influenced by G_iP, respectively. Thus, the multipliers α_{11} and α_{12} describe autoregulatory interactions mediated by G_1P, whereas α_{13},α_{14},α_{21} and α_{22} determine feedforward and feedback loops between G_1P and G_2P. Parameters V_1, V_2 and V_3, V_4 are the maximal rates of GEF and GAP-catalyzed reactions at the first and second layers, respectively, and K_1, K_2, K_3 and K_4 are the corresponding Michaelis constants. Assuming general hyperbolic modifier kinetics, each multiplier (α_{ij}) has the same functional form $F(a_{ij}, G_iP, K_{ij})$ [36],

$$\alpha_{ij} = F(a_{ij}, G_iP, K_{ij}) = \frac{1 + a_{ij}\cdot G_iP/K_{ij}}{1 + G_iP/K_{ij}}, \quad i = 1, 2; \quad j = 1, 2, 3, 4 \qquad (2).$$

The coefficient $a_{ij} > 1$ indicates activation; $a_{ij} < 1$ inhibition; and $a_{ij} = 1$ denotes the absence of regulatory interactions, in which case the function F equals 1, K_{ij} is the activation or inhibition constant. Note that $\alpha_{23} = 1$ and $\alpha_{24} = 1$, since we consider cascades with a single autoregulatory loop mediated by G_1P.

It is convenient to use the normalized (dimensionless) concentrations, $g_1p(t)$, $g_2p(t)$, which represent active GTPase fractions, $g_1p = G_1P/G_1^{tot}$, $g_2p = G_2P/G_2^{tot}$. This simplifies Eqs. 1 and 2, as follows,

$$\frac{dg_1 p}{dt} = \alpha_{11}\alpha_{21}u_1 - \alpha_{12}\alpha_{22}u_2, \quad u_1 = r_1 \frac{(1-g_1 p)/m_1}{1+(1-g_1 p)/m_1}, \quad u_2 = r_2 \frac{g_1 p/m_2}{1+g_1 p/m_2}$$

$$\frac{dg_2 p}{dt} = \alpha_{13}u_3 - \alpha_{14}u_4, \qquad u_3 = r_3 \frac{(1-g_2 p)/m_3}{1+(1-g_2 p)/m_3}, \quad u_4 = r_4 \frac{g_2 p/m_4}{1+g_2 p/m_4} \qquad (3).$$

$$m_1 = K_1/G_1^{tot},\ m_2 = K_2/G_1^{tot},\ m_3 = K_3/G_2^{tot},\ m_4 = K_4/G_2^{tot},$$

$$r_1 = V_1/G_1^{tot},\ r_2 = V_2/G_1^{tot},\ r_3 = V_3/G_2^{tot},\ r_4 = V_4/G_2^{tot}$$

Here m_i denote the dimensionless Michaelis constants (normalized by the total GTPase abundances, G_1^{tot} and G_2^{tot}), and r_i are the ratios of the maximal rates and the total GTPase abundances. Each of the 64 different molecular designs (Fig. 2) is fully specified by the dimensionless multipliers α_{ij} (see Eq. 2),

$$\alpha_{ij}(g_i p) = \frac{1 + a_{ij} \cdot g_i p / m_{ij}}{1 + g_i p / m_{ij}} \qquad (4).$$

Here $m_{ij} = K_{ij}/G_i^{tot}$, and for the coefficients a_{ij} and m_{ij}, indices *i* (*i* =1, 2) and *j* (*j* =1, …, 4) indicate a GTPase (G_iP) and reaction *j* that is activated or inhibited by that GTPase. For instance, $\alpha_{11} \neq 1$ shows that G_1P (active GTPase at the upper layer) stimulates or inhibits its own GEF. If $\alpha_{12} \neq 1$, then G_1P stimulates or inhibits its own GAP. For *j* = 1 or 2, $\alpha_{2j} \neq 1$ specifies that G_2P (active GTPase at the lower layer) feeds back and affects GEF (*j* = 1) or GAP (*j*=2), respectively, at the upper level; for *j* = 3 or 4, $\alpha_{1j} \neq 1$ shows that G_1P at the upper layer feeds forward and affects GEF (*j* = 3) or GAP (*j*=4) at the downstream level. Therefore, any particular cascade design from the 64 total is described by three pairs of the dimensionless multipliers $(\alpha_{11}, \alpha_{12})$, $(\alpha_{21}, \alpha_{22})$, $(\alpha_{13}, \alpha_{14})$, where in each pair one multiplier equals 1 (and the other does not). Note that completely dimensionless ODEs can be obtained by introducing dimensionless time ($\tau = r_1 t$). Although this would reduce the number of parameters by one (giving the minimal number of independent parameter combinations), perturbations to the rate of a single step (V_1) would change multiple parameter combinations. Thus, we wish to exploit Eqs. 3 and 4 to classify cascade dynamics.

Equations presented in the left column of Table 1 govern the temporal dynamics of all 8 different cascades within each topology group (I - VIII) shown in Fig. 1b. For instance, kinetic equations for the 8 different group I cascades (shown in Fig. 2) can be obtained from Table 1 by assigning $\alpha_{11} > 1$ *or* $\alpha_{12} < 1$, and $\alpha_{21} < 1$ *or* $\alpha_{22} > 1$, and $\alpha_{13} > 1$ *or* $\alpha_{14} < 1$. Likewise, 8 different cascade circuitries that comprise group III are also described by Table 1; the only difference with group I is that for cascades in group III, $\alpha_{21} > 1$ *or* $\alpha_{22} < 1$. This difference corresponds to the replacement of negative feedback from G_2P in the group I circuitries by positive feedback in the group III circuitries (SI1 specifies each cascade group I - VIII in terms of the values of the dimensional multipliers α_{ij}).

Relationships between regulatory loop parameters that lead to identical nullclines and steady states for all eight different cascade designs within each group I - VIII.

For cascade designs 2 - 8, Table 1 presents the relationships between the kinetic constants of regulatory loops, which guarantee that the nullclines and steady states for each of these designs are identical to that of design 1. Here we derive such relationships for design 2 (the corresponding derivations for designs 3 - 8 are given in Supplementary material 2). Equating the time derivatives in Table 1 to zero, we find that the corresponding nullcline equations for designs 2 and 1 will be identical, if and only if,

$$\alpha_{22}^{(2)}(g_2 p) = 1/\alpha_{21}^{(1)}(g_2 p) \qquad (5),$$

where superscripts (1) and (2) indicate the design number. Substituting Eq. 4 into Eq. 5, we obtain,

$$\frac{1 + a_{21}^{(1)} g_2 p / m_{21}^{(1)}}{1 + g_2 p / m_{21}^{(1)}} = \frac{1 + g_2 p / m_{22}^{(2)}}{1 + a_{22}^{(2)} g_2 p / m_{22}^{(2)}} \qquad (6)$$

Since Eq. 6 must be satisfied for any g_2p value, this results in the following constraint between the kinetic constants of G_2P-mediated activation or inhibition of G_1P for cascade designs 1 and 2,

$$a_{22}^{(2)} = 1/a_{21}^{(1)},\ m_{22}^{(2)} = m_{21}^{(1)}/a_{21}^{(1)} \qquad (7)$$

Eq. 7 guarantees the identical nullclines and steady states for designs 2 and 1 within any of the cascade groups I - VIII shown in Fig. 1b.

Table 1. Relationships between kinetic parameters that enable the identity of steady states for molecular designs 1 - 8 within each topology group (I – VIII) in Fig.2.

Equations governing the temporal dynamics for each kinetic design	Relationships between kinetic parameters*
Design 1 $dg_1 p/dt = \alpha_{11}\alpha_{21}u_1 - u_2$ $dg_2 p/dt = \alpha_{13}u_3 - u_4$	
Design 2 $dg_1 p/dt = \alpha_{11}u_1 - \alpha_{22}u_2$ $dg_2 p/dt = \alpha_{13}u_3 - u_4$	Designs 2 and 1 $a_{22}^{(2)} = 1/a_{21}^{(1)},\ m_{22}^{(2)} = m_{21}^{(1)}/a_{21}^{(1)}$
Design 3 $dg_1 p/dt = u_1 - \alpha_{12}\alpha_{22}u_2$ $dg_2 p/dt = \alpha_{13}u_3 - u_4$	Designs 3 and 1 $a_{12}^{(3)} = 1/a_{11}^{(1)}, m_{12}^{(3)} = m_{11}^{(1)}/a_{11}^{(1)}$ $a_{22}^{(3)} = 1/a_{21}^{(1)}, m_{22}^{(3)} = m_{21}^{(1)}/a_{21}^{(1)}$
Design 4 $dg_1 p/dt = \alpha_{21}u_1 - \alpha_{12}u_2$ $dg_2 p/dt = \alpha_{13}u_3 - u_4$	Designs 4 and 1 $a_{12}^{(4)} = 1/a_{11}^{(1)},\ m_{12}^{(4)} = m_{11}^{(1)}/a_{11}^{(1)}$
Design 5 $dg_1 p/dt = \alpha_{11}\alpha_{21}u_1 - u_2$ $dg_2 p/dt = u_3 - \alpha_{14}u_4$	Designs 5 and 1 $a_{14}^{(5)} = 1/a_{13}^{(1)},\ m_{14}^{(5)} = m_{13}^{(1)}/a_{13}^{(1)}$
Design 6 $dg_1 p/dt = \alpha_{11}u_1 - \alpha_{22}u_2$ $dg_2 p/dt = u_3 - \alpha_{14}u_4$	Designs 6 and 1 $a_{14}^{(6)} = 1/a_{13}^{(1)}, m_{14}^{(6)} = m_{13}^{(1)}/a_{13}^{(1)}$ $a_{22}^{(6)} = 1/a_{21}^{(1)}, m_{22}^{(6)} = m_{21}^{(1)}/a_{21}^{(1)}$
Design 7 $dg_1 p/dt = u_1 - \alpha_{12}\alpha_{22}u_2$ $dg_2 p/dt = u_3 - \alpha_{14}u_4$	Designs 7 and 1 $a_{14}^{(7)} = 1/a_{13}^{(1)}, m_{14}^{(7)} = m_{13}^{(1)}/a_{13}^{(1)}$ $a_{12}^{(7)} = 1/a_{11}^{(1)}, m_{12}^{(7)} = m_{11}^{(1)}/a_{11}^{(1)}$ $a_{22}^{(7)} = 1/a_{21}^{(1)},\ m_{22}^{(7)} = m_{21}^{(1)}/a_{21}^{(1)}$
Design 8 $dg_1 p/dt = \alpha_{21}u_1 - \alpha_{12}u_2$ $dg_2 p/dt = u_3 - \alpha_{14}u_4$	Designs 8 and 1 $a_{14}^{(8)} = 1/a_{13}^{(1)}, m_{14}^{(8)} = m_{13}^{(1)}/a_{13}^{(1)}$ $a_{12}^{(8)} = 1/a_{11}^{(1)},\ m_{12}^{(8)} = m_{11}^{(1)}/a_{11}^{(1)}$

*****Superscripts in the right column indicate different designs. The parameters in the left column (see Eq. 3), which are not explicitly present in the right column are equal to the corresponding parameters of design 1.

Modeling GTPase cascade signaling in space and time.

We consider a simple, one-dimensional geometry with the Cartesian spatial coordinate (X) which is confined between 0 and L (a typical cell size). Assuming that cascade GTPases (including both GDP- and GTP-bound forms) have the same the diffusion coefficients (D_G), the spatiotemporal dynamics of any of the 64 cascades is described, as follows,

$$\begin{aligned} \frac{\partial g_1 p(x,t)}{\partial t} &= \alpha_{11}\alpha_{21}u_1 - \alpha_{12}\alpha_{22}u_2 + D\Delta g_1 p \\ \frac{\partial g_2 p(x,t)}{\partial t} &= \alpha_{13}u_3 - \alpha_{14}u_4 + D\Delta g_2 p \end{aligned} \qquad (8)$$

$$D = \frac{D_G}{L^2},\ \Delta = \frac{\partial^2}{\partial x^2},\quad x = X/L$$

$$\left.\frac{\partial g_i p}{\partial x}\right|_{x=0} = \left.\frac{\partial g_i p}{\partial x}\right|_{x=1} = 0, \quad i = 1,2 \qquad (9)$$

Here D is the normalized diffusion coefficient, x is the normalized, dimensionless spatial coordinate, and the boundary conditions imply there is no diffusive flux of active GTPase concentrations at either pole ($x = 0$ and $x = 1$).

The numerical simulations were carried out using the Euler method with Neumann boundary conditions (Eq. 22) in the interval $x \in [0, 1]$, time step $2\cdot10^{-4}$ s and space step $5\cdot10^{-3}$. $D = 0.015$ s^{-1} (which corresponds to the GTPase diffusion coefficient D_G of 6 to 10 μm^2·s^{-1} [65]) and the cell size of $L = 20$ to about 26 μm, respectively. The initial conditions (unperturbed) corresponded to a stable, spatially homogeneous steady state of the GTPase fractions, $g_1p(x,0) = g_1p_{ss}$, $g_2p(x,0) = g_2p_{ss}$, for $0 \le x \le 1$. The initial perturbations were confined within a small spatial area, $0 \le x \le 0.03$ (for all kinetic parameters and stationary values, see figure legends and SI).

Heterogeneous spatial distribution of GAP/GEF activities

Let GAP_2 be phosphorylated by a membrane kinase (at $x = 0$) and dephosphorylated by a cytoplasmic phosphatase. Assuming that the phosphorylated GAP_2 form has a higher catalytic activity and the phosphatase is far from saturation, the dependence of constitutive GAP_2 activity (which is described by the parameter r_4, see Eq. 3) on the spatial coordinate x can be approximated as follows [13],

$$r_4(x) = r_4(1) + (r_4(0) - r_4(1)) \cdot \left(\frac{e^{\eta x} + e^{2\eta} e^{-\eta x}}{1 + e^{2\eta}} \right) \qquad (10)$$

Here the dimensionless parameter η is expressed in terms of the GAP_2 diffusion coefficient (D_G), the cell size (L) and the apparent first-order rate constant of the phosphatase (k_p), as follows, $\eta = \sqrt{k_p /(D_G / L^2)}$. The selected value of $\eta = 6.7$ corresponds, for instance, to the following parameters, $D_G = 10\ \mu m^2 \cdot s^{-1}$, $L = 25.8\ \mu m$, $k_p = 0.67\ s^{-1}$.

Spatiotemporal dynamics of active GTPase fractions in a three-tired cascade

For a three-tier cascade shown in Fig. 7, the reaction-diffusion equations that govern the spatiotemporal dynamics of active GTPase fractions, $g_1p(x,t)$, $g_2p(x,t)$ and $g_3p(x,t)$, are presented as follows (see Eqs. 8 and 9),

$$\begin{aligned}
&\frac{\partial g_1 p}{dt} = \alpha_{21} u_1 - u_2 + D\Delta g_1 p, && u_1 = r_1 \frac{(1-g_1 p)/m_1}{1+(1-g_1 p)/m_1}, \quad u_2 = r_2 \frac{g_1 p/m_2}{1+g_1 p/m_2} \\
&\frac{\partial g_2 p}{dt} = \alpha_{13} u_3 - \alpha_{34} u_4 + D\Delta g_2 p, && u_3 = r_3 \frac{(1-g_2 p)/m_3}{1+(1-g_2 p)/m_3}, \quad u_4 = r_4 \frac{g_2 p/m_4}{1+g_2 p/m_4} \\
&\frac{\partial g_3 p}{dt} = \alpha_{25} u_5 - u_5 + D\Delta g_3 p, && u_5 = r_5 \frac{(1-g_3 p)/m_5}{1+(1-g_3 p)/m_5}, \quad u_6 = r_6 \frac{g_3 p/m_6}{1+g_3 p/m_6}
\end{aligned} \tag{11}$$

$$\left.\frac{\partial g_i p}{\partial x}\right|_{x=0} = \left.\frac{\partial g_i p}{\partial x}\right|_{x=1} = 0, \quad i = 1,\ 2,\ 3.$$

Here we use the same notations as in Eqs. 8 and 9; the dimensionless multipliers α_{ij} are given in Eq.4 where $i = 1, 2, 3$; $j = 1, 2, 3, 4, 5, 6$.

Acknowledgement. Supported by Science Foundation Ireland under Grant No. 06/CE/B1129 and NIH grant GM059570.

Conflict of Interest. The authors do not have any competing commercial interests.

Notes and References

Electronic Supplementary Information (ESI) is available on the Journal website.

1. L. E. Goldfinger, *Mol Biosyst*, 2008, **4**, 293-299.
2. Y. Takai, T. Sasaki and T. Matozaki, *Physiol Rev*, 2001, **81**, 153-208.
3. A. J. Ridley, *J Cell Sci*, 2001, **114**, 2713-2722.
4. D. J. Mackay and A. Hall, *J Biol Chem*, 1998, **273**, 20685-20688.
5. E. Giniger, *Differentiation*, 2002, **70**, 385-396.
6. J. Stelling and B. N. Kholodenko, *J Math Biol*, 2008.
7. P. Del Conte-Zerial, L. Brusch, J. C. Rink, C. Collinet, Y. Kalaidzidis, M. Zerial and A. Deutsch, *Mol Syst Biol*, 2008, **4**, 206.

8. A. B. Jaffe and A. Hall, *Annu Rev Cell Dev Biol*, 2005, **21**, 247-269.
9. S. J. Heasman and A. J. Ridley, *Nat Rev Mol Cell Biol*, 2008, **9**, 690-701.
10. E. E. Sander, J. P. ten Klooster, S. van Delft, R. A. van der Kammen and J. G. Collard, *J Cell Biol*, 1999, **147**, 1009-1022.
11. K. Burridge and K. Wennerberg, *Cell*, 2004, **116**, 167-179.
12. M. Machacek, L. Hodgson, C. Welch, H. Elliott, O. Pertz, P. Nalbant, A. Abell, G. L. Johnson, K. M. Hahn and G. Danuser, *Nature*, 2009, **461**, 99-103.
13. B. N. Kholodenko, *Nat Rev Mol Cell Biol*, 2006, **7**, 165-176.
14. Y. Sakumura, Y. Tsukada, N. Yamamoto and S. Ishii, *Biophys J*, 2005, **89**, 812-822.
15. A. Jilkine, A. F. Maree and L. Edelstein-Keshet, *Bull Math Biol*, 2007, **69**, 1943-1978.
16. A. S. Howell, N. S. Savage, S. A. Johnson, I. Bose, A. W. Wagner, T. R. Zyla, H. F. Nijhout, M. C. Reed, A. B. Goryachev and D. J. Lew, *Cell*, 2009, **139**, 731-743.
17. Y. Mori, A. Jilkine and L. Edelstein-Keshet, *Biophys J*, 2008, **94**, 3684-3697.
18. J. R. Kim, Y. Yoon and K. H. Cho, *Biophys J*, 2008, **94**, 359-365.
19. B. N. Kholodenko, J. F. Hancock and W. Kolch, *Nat Rev Mol Cell Biol*, 2010, **11**, 414-426.
20. T. Nakakuki, M. R. Birtwistle, Y. Saeki, N. Yumoto, K. Ide, T. Nagashima, L. Brusch, B. A. Ogunnaike, M. Okada-Hatakeyama and B. N. Kholodenko, *Cell*, 2010, **141**, 884-896.
21. G. C. Brown and B. N. Kholodenko, *FEBS Lett*, 1999, **457**, 452-454.
22. B. N. Kholodenko, *FEBS Lett*, 2009, **583**, 4006-4012.
23. P. Kalab, K. Weis and R. Heald, *Science*, 2002, **295**, 2452-2456.
24. J. Munoz-Garcia, B. N. Kholodenko and Z. Neufeld, *Biophys J*, 2010, **99**, 59-66.
25. J. Munoz-Garcia, Z. Neufeld and B. N. Kholodenko, *PLoS Comput Biol*, 2009, **5**, e1000330.
26. M. Caudron, G. Bunt, P. Bastiaens and E. Karsenti, *Science*, 2005, **309**, 1373-1376.
27. C. A. Athale, A. Dinarina, M. Mora-Coral, C. Pugieux, F. Nedelec and E. Karsenti, *Science*, 2008, **322**, 1243-1247.
28. C. Tischer and P. I. Bastiaens, *Nat Rev Mol Cell Biol*, 2003, **4**, 971-974.
29. N. I. Markevich, M. A. Tsyganov, J. B. Hoek and B. N. Kholodenko, *Mol Syst Biol*, 2006, **2**, 61.
30. J. Munoz-Garcia and B. N. Kholodenko, *Biochem Soc Trans*, 2010, **38**, 1235-1241.
31. A. M. Zhabotinsky and A. N. Zaikin, *J Theor Biol*, 1973, **40**, 45-61.
32. J. D. Murray, *Mathematical Biology*, Springer, New York, 2001.
33. A. R. Reynolds, C. Tischer, P. J. Verveer, O. Rocks and P. I. Bastiaens, *Nat Cell Biol*, 2003, **5**, 447-453.
34. T. S. Freedman, H. Sondermann, G. D. Friedland, T. Kortemme, D. Bar-Sagi, S. Marqusee and J. Kuriyan, *Proc Natl Acad Sci U S A*, 2006, **103**, 16692-16697.
35. Q. Lin, W. Yang, D. Baird, Q. Feng and R. A. Cerione, *J Biol Chem*, 2006, **281**, 35253-35262.
36. A. Cornish-Bowden, *Portland Press, London*, 1995.
37. J. E. Ferrell, Jr., *Curr Opin Cell Biol*, 2002, **14**, 140-148.
38. U. S. Bhalla, P. T. Ram and R. Iyengar, *Science*, 2002, **297**, 1018-1023.
39. N. I. Markevich, J. B. Hoek and B. N. Kholodenko, *J Cell Biol*, 2004, **164**, 353-359.
40. J. Das, M. Ho, J. Zikherman, C. Govern, M. Yang, A. Weiss, A. K. Chakraborty and J. P. Roose, *Cell*, 2009, **136**, 337-351.
41. J. J. Tyson and B. Novak, *Curr Biol*, 2008, **18**, R759-R768.
42. J. U. Hwang, Y. Gu, Y. J. Lee and Z. Yang, *Mol Biol Cell*, 2005, **16**, 5385-5399.
43. L. Qiao, R. B. Nachbar, I. G. Kevrekidis and S. Y. Shvartsman, *PLoS Comput Biol*, 2007, **3**, 1819-1826.
44. A. Goldbeter, *Nature*, 2002, **420**, 238-245.
45. T. Y. Tsai, Y. S. Choi, W. Ma, J. R. Pomerening, C. Tang and J. E. Ferrell, Jr., *Science*, 2008, **321**, 126-129.
46. N. P. Kaimachnikov and B. N. Kholodenko, *Febs J*, 2009, **276**, 4102-4118.
47. B. N. Kholodenko, *J Exp Biol*, 2003, **206**, 2073-2082.

48. I. A. Yudushkin, A. Schleifenbaum, A. Kinkhabwala, B. G. Neel, C. Schultz and P. I. Bastiaens, *Science*, 2007, **315**, 115-119.
49. C. I. Maeder, M. A. Hink, A. Kinkhabwala, R. Mayr, P. I. Bastiaens and M. Knop, *Nat Cell Biol*, 2007, **9**, 1319-1326.
50. S. R. Neves and R. Iyengar, *J Biol Chem*, 2009, **284**, 5445-5449.
51. M. Sabouri-Ghomi, Y. Wu, K. Hahn and G. Danuser, *Curr Opin Cell Biol*, 2008, **20**, 541-550.
52. H. L. Swinney and V. I. Krinsky, *Waves and Patterns in Chemical and Biological Media (North-Holland, Amsterdam, 1991)*, 1991.
53. A. J. Ridley, M. A. Schwartz, K. Burridge, R. A. Firtel, M. H. Ginsberg, G. Borisy, J. T. Parsons and A. R. Horwitz, *Science*, 2003, **302**, 1704-1709.
54. K. Rottner, A. Hall and J. V. Small, *Curr Biol*, 1999, **9**, 640-648.
55. A. S. Nimnual, L. J. Taylor and D. Bar-Sagi, *Nat Cell Biol*, 2003, **5**, 236-241.
56. Z. Li, C. D. Aizenman and H. T. Cline, *Neuron*, 2002, **33**, 741-750.
57. B. N. Kholodenko, *Nat Cell Biol*, 2007, **9**, 247-249.
58. S. D. Santos, P. J. Verveer and P. I. Bastiaens, *Nat Cell Biol*, 2007, **9**, 324-330.
59. J. J. Tyson, K. C. Chen and B. Novak, *Current Opinion in Cell Biology*, 2003, **15**, 221-231.
60. B. Novak and J. J. Tyson, *Nat Rev Mol Cell Biol*, 2008, **9**, 981-991.
61. F. N. Leeuwen, H. E. Kain, R. A. Kammen, F. Michiels, O. W. Kranenburg and J. G. Collard, *J Cell Biol*, 1997, **139**, 797-807.
62. B. N. Kholodenko, *Eur J Biochem*, 2000, **267**, 1583-1588.
63. Z. Hilioti, W. Sabbagh, Jr., S. Paliwal, A. Bergmann, M. D. Goncalves, L. Bardwell and A. Levchenko, *Curr Biol*, 2008, **18**, 1700-1706.
64. H. Shankaran, D. L. Ippolito, W. B. Chrisler, H. Resat, N. Bollinger, L. K. Opresko and H. S. Wiley, *Mol Syst Biol*, 2009, **5**, 332.
65. D. Gorlich, M. J. Seewald and K. Ribbeck, *Embo J*, 2003, **22**, 1088-1100.

Figure Legends

Fig. 1. Regulatory interactions between GTPases create 128 different molecular topologies for a two-layer cascade.

a. General cascade interaction structure. GEF- and GAP-catalyzed reactions are shown as kinetically irreversible transitions between different GTPase forms, the reaction rates are denoted by v_i (i is the reaction number). Lines ending with stars indicate regulatory interactions of active GTPase forms, G_1P and G_2P, with GEFs and GAPs at the same layer or other cascade layer. Solid and dashed lines show all potential regulatory circuitries. **b**. Eight "influence" diagrams describing 64 possible molecular topologies. Active GTPase forms are shown by bold dots. At the top layer, G_1P activates or inhibits its own GEF or GAP. Red lines with arrows and blue lines with blunt ends show activating and inhibitory loops, respectively. Since every red loop corresponds to either GEF activation or GAP inhibition, and every blue loop corresponds to GEF inhibition or GAP activation, each influence diagram generates eight different molecular wiring designs, which form a group. These eight groups (I - VIII) embrace 64 different molecular circuitries in total. Note that 64 mirror symmetry circuits are generated when auto-activation and auto-inhibition loops are mediated by G_2P.

Fig. 2. Eight kinetic designs comprising group I of two-layer GTPase cascades. Dimensionless multipliers α_{ij} indicate the influences of active GTPase (subscript i) on GEFs (rates v_1 and v_3) and GAPs (v_2 and v_4), subscript j denotes the affected enzyme rate. In regulatory loops, arrows and blunt ends show activation ($a_{ij} > 1$) and inhibition ($a_{ij} < 1$), respectively. Eight group I cascades are represented by one influence diagram in Fig. 1b.

Fig. 3. Bistability and hysteresis in GTPase cascades comprising molecular topology groups I - VI. Panels in the left column show the g_1p-nullcline (purple) and g_2p-nullcline (green) on the (g_1p, g_2p) plane for cascades in groups I - VI. The nullclines intersect in three points where S_1 and S_2 are stable steady states and U is an unstable steady state. Panels in the right column show hysteretic behavior of steady-state responses of active GTPase fractions, g_1p (purple) and g_2p (green) to the changes in the input GEF_1 activity. Dotted lines correspond to unstable steady states located at the intermediate branch of the curve between turning points P_1 and P_2 (marked bold). The dependencies of steady-state responses on parameters are identical for all eight cascades within a group, if the proper relationships between kinetic parameters of different cascades are satisfied (Table 1, Methods). Hysteresis curves are calculated for topology design 1 in each group. The kinetic parameters and the values of active GTPase fractions in the steady states S_1 and S_2 are given in SI (Table S1).

Fig.4. Oscillatory dynamics and overshoot transitions of GTPase activities.

(**a-d**) ***Sustained oscillations of active GTPases***. Oscillations of active GTPase fractions (g_1p, purple and g_2p, green) are shown for cascade designs 1 and 5 of group I (**a**, **b**) and group II (**c**, **d**). Parameter values are given in Table S2. **(e-h)** ***Excitable behavior of GTPase cascades.*** Responses of active GTPase fractions to perturbations of different amplitudes are shown for cascade designs 5 (group I) and 1 (group II). Initially, a cascade resides in a stable, but excitable steady state. Two different initial steady states for design 5 (**e, f)** and design 1 (**g, h**) correspond to different GEF_2 activities, as indicated in Table S2 that presents the values of parameters and stationary GTPase fractions. At time $t = 3$ sec (marked by black arrow), the steady-state concentration (g_1p) of the active GTPase at the first level is perturbed. Sub-threshold perturbations cause small responses shown by dashed lines. Over-threshold perturbations cause large overshoot responses where the active GTPase fractions can significantly increase or decrease, generating temporal pulses of GTPase activities (threshold values of g_1p perturbation amplitudes are marked by red arrows). Note that the changes in the cascade dynamics (excitable responses (**e-h**) versus oscillatory (**a-d**) behaviors) are brought about by a variation of a single parameter (GEF_2 activity). The difference between the kinetic parameters of different designs that are shown in panels **a-h** is specified by the relationships given in Table I (Methods).

Fig.5. Travelling waves of global switches and pulses of GTPase (de)activation.

Initially, a cascade resides in a stable, spatially homogeneous steady state where stationary GTPase activities do not depend on the spatial coordinate, x, which is normalized by the cell size ($0 \le x \le 1$, see Methods). Spatial profiles of the active GTPase fraction $g_1p(x, t)$ are shown using different colors for selected time points (seconds), following the initial perturbation (at time $t = 0$, brown line) that is confined within a small spatial area, $0 \le x \le 0.03$. Upper panels show trigger waves (global switches) of g_1p activation (**a**) and g_1p deactivation (**b**), and lower panels show excitable waves of g_1p activation pulses (**c**) and g_1p deactivation pulses (**d**) travelling through the cell. Arrows show the direction of wave propagation. For bistable (**a, b**) and excitable (**c, d**) cascades, the kinetic parameters and the initial, spatially homogeneous steady state values of active GTPase fractions are presented in Tables S1 and S2, respectively.

Fig. 6. Propagation of periodic pulses through spatially heterogeneous media.

The GAP_2 constitutive activity of a cascade decreases with the distance (x) from the plasma membrane as governed by Eq. 10 (Methods) and illustrated in Fig. S5. (**a**) Close to the membrane ($x \approx 0$), active GTPase fractions (g_1p, purple and g_2p, green) oscillate. A decrease in GAP_2 activity father into the cell interior brings about the change in the cascade dynamics; oscillatory behavior is no longer observed, whereas excitable behavior emerges at $x \approx 0.2$ (the Hopf bifurcation point). (**b**) A pulse-like wave propagating through a cell is shown for a selected time window (3.6 - 4.8 s), using different colors for different time

moments. The arrow shows the direction of the wave propagation. (**c**) A 3-D presentation of propagating waves of periodic GTPase activity pulses driven by oscillating GTPase activities near the membrane. Kinetic parameters and the initial, spatially homogeneous steady state GTPase activities are given in Table S2.

Fig. 7. An overview of possible spatiotemporal behaviors of all topology groups for two-layer GTPase cascades. Nullclines, the time evolution and snapshots of the spatial profiles for distinctive spatiotemporal regimes are shown for the corresponding sets of topology groups. Different colors are used to indicate different time moments for the spatial profile snapshots and to show the time evolution for the different initial conditions (pre-existing GTPase activities in the cascade).

Fig. 8. Spatiotemporal dynamics of active GTPase fractions for a three-tired cascade.
a. Kinetic design (at the left) and reduced "influence" diagram of a cascade. Arrows and blunt ends show activation and inhibition, respectively. **b.** Oscillations of active GTPase fractions, g_1p (blue), g_2p (purple) and g_3p (green) for a spatially homogenous system. Trigger waves (**c**) and pulse-like waves (**d**) of GTPase activation. Spatial profiles of the active GTPase fractions are shown for selected time points following the initial perturbation, (**c)** t=3 sec, (**d**) t=0.9 sec. The arrows show the direction of wave propagation. Kinetic parameters, the initial GTPase activities, corresponding to the spatially homogeneous steady states, and the perturbation amplitudes are given in Table S3.

Electronic Supplementary Information

The Topology Design Principles that Determine the Spatiotemporal Dynamics of G-protein Cascades.

Mikhail A. Tsyganov[1,2], Walter Kolch[2] and Boris N. Kholodenko[2,3*]

[1]Institute of Theoretical and Experimental Biophysics, Pushchino, Moscow Region, Russia

[2]Systems Biology Ireland, University College Dublin, Belfield, Dublin 4, Ireland,

[3]Thomas Jefferson University, Department of Pathology, Anatomy, and Cell Biology, Philadelphia, PA 19107, USA

Supplementary Figures.

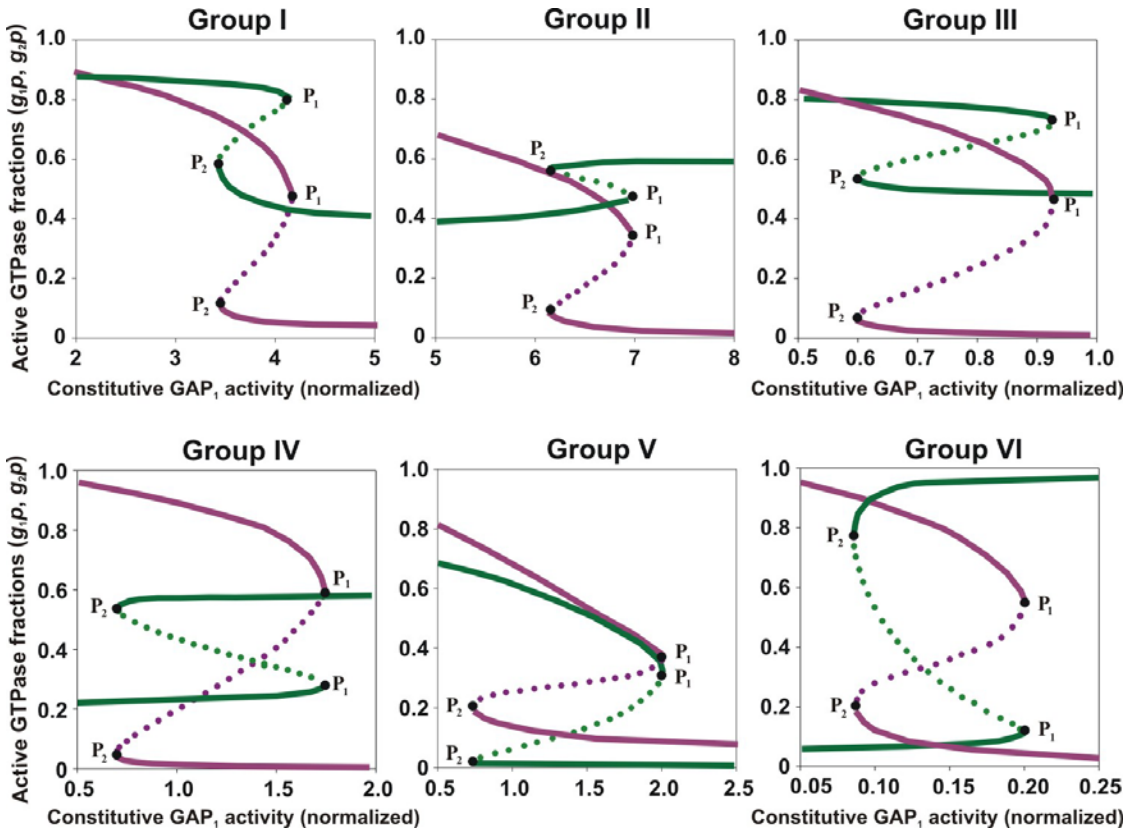

Fig. S1. Bistability and hysteresis in GTPase cascades in groups I - VI: responses to gradual changes in GAP$_1$ concentrations. Hysteretic behavior of the steady-state responses of active GTPase fractions, g_1p (purple) and g_2p (green), to the changes in the input GAP$_1$ activity (parameter r_2) are shown. Dotted lines correspond to unstable steady states located at the intermediate branch of the curve between turning points P_1 and P_2 (marked bold). The dependencies of steady-state responses on parameters are identical for all eight designs within a group, if the relationships between kinetic parameters enabling the identity of steady states are satisfied (see Table 1, Methods). For each group I - VI, the hysteresis curves are calculated for topology design 1, whose kinetic parameters are given in Table S1 where parameter r_2 is varied in the ranges shown (s^{-1}). Note that the stationary, active GTPase fractions behave similarly when the input GEF or GAP activity is changed by altering the strength of the autocatalytic loop (given by values of the multiplies α_{11} and α_{12}, Eq.4, Methods) rather than by changing the maximal rate r_1 or r_2.

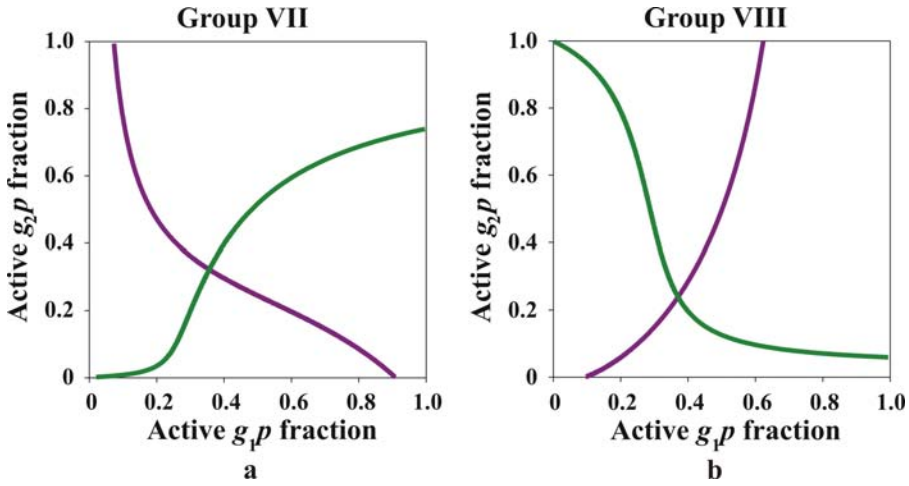

Fig.S2. Typical nullcline shapes for 16 cascade topologies that comprise VII and VIII groups. (**a**). Group VII. The g_1p-nullcline (purple) is a monotone decreasing function of g_1p and the g_2p-nullcline (green) is a monotone increasing function of g_1p, which cannot intersect at more than one point. (**b**). Group VIII. The g_1p-nullcline (purple) is a monotone increasing function of g_1p and the g_2p-nullcline (green) is a monotone decreasing function of g_1p, and, therefore, these two nullclines cannot intersect at more than one point. Kinetic parameters are the following: (**a**) r_1= 1, r_2= 0.13, r_3= 10, r_4= 30 (s^{-1}), m_1= 0.4, m_2=0.09, m_3= 2, m_4= 0.01, a_{11}= 0.6, m_{11}= 0.1, a_{13}= 100, m_{13}= 3, a_{21}= 0.01, m_{21}= 0.1; (**b**) r_1= 1, r_2= 1.5, r_3= 1, r_4= 0.01 (s^{-1}), m_1= 1, m_2=5, m_3= 0.1, m_4= 0.05, a_{11}= 0.01, m_{11}= 0.005, a_{13}= 0.004, m_{13}= 0.002, a_{21}= 100, m_{21}= 2.

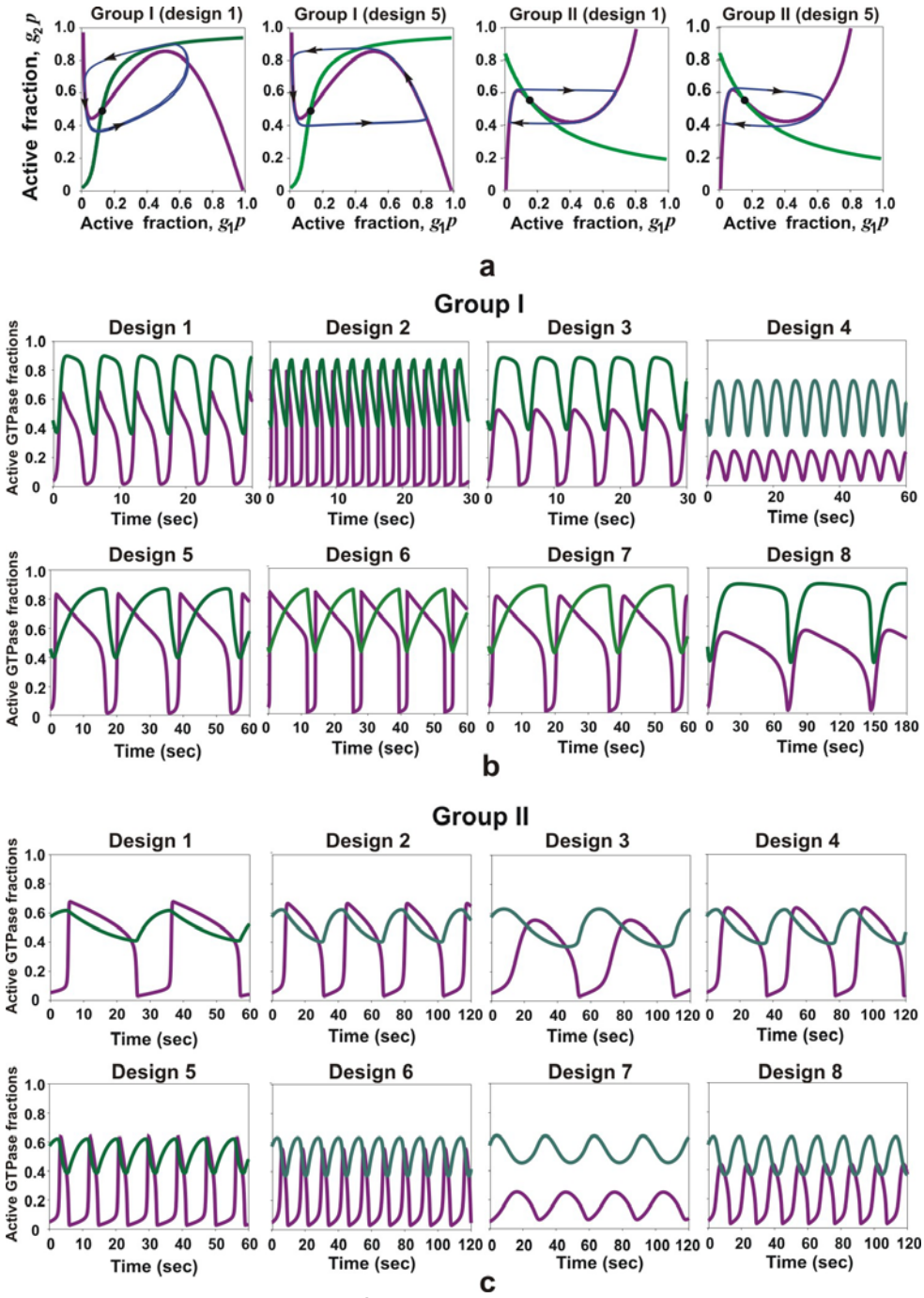

Fig. S3. Oscillatory regimes of 16 cascades comprising groups I and II. (a) The g_1p-nullclines (purple, N-mirror shaped, group I, and N-shaped, group II) and the g_2p-nullclines (green, monotone) intersect at a single point (marked in bold) corresponding to an unstable steady state. The limit cycle trajectories (blue) on the plane (g_1p, g_2p) are shown for kinetic designs 1 and 5. Arrows indicate the direction of motion. (**b**, **c**) Sustained oscillations of active GTPase fractions (g_1p, purple and g_2p, green) are shown for all kinetic designs comprising groups I and II. Kinetic parameters are presented in Table S2 for design 1, and the parameter value relationships for other designs are specified in Table 1 (Methods). For illustrative purposes, for design 4 in group I the constitutive GEF_1 and GAP_1 activities were increased by a factor of 2 compared to the activities presented in Table S2, as follows, r_1= 10, r_2= 8 (s^{-1}).

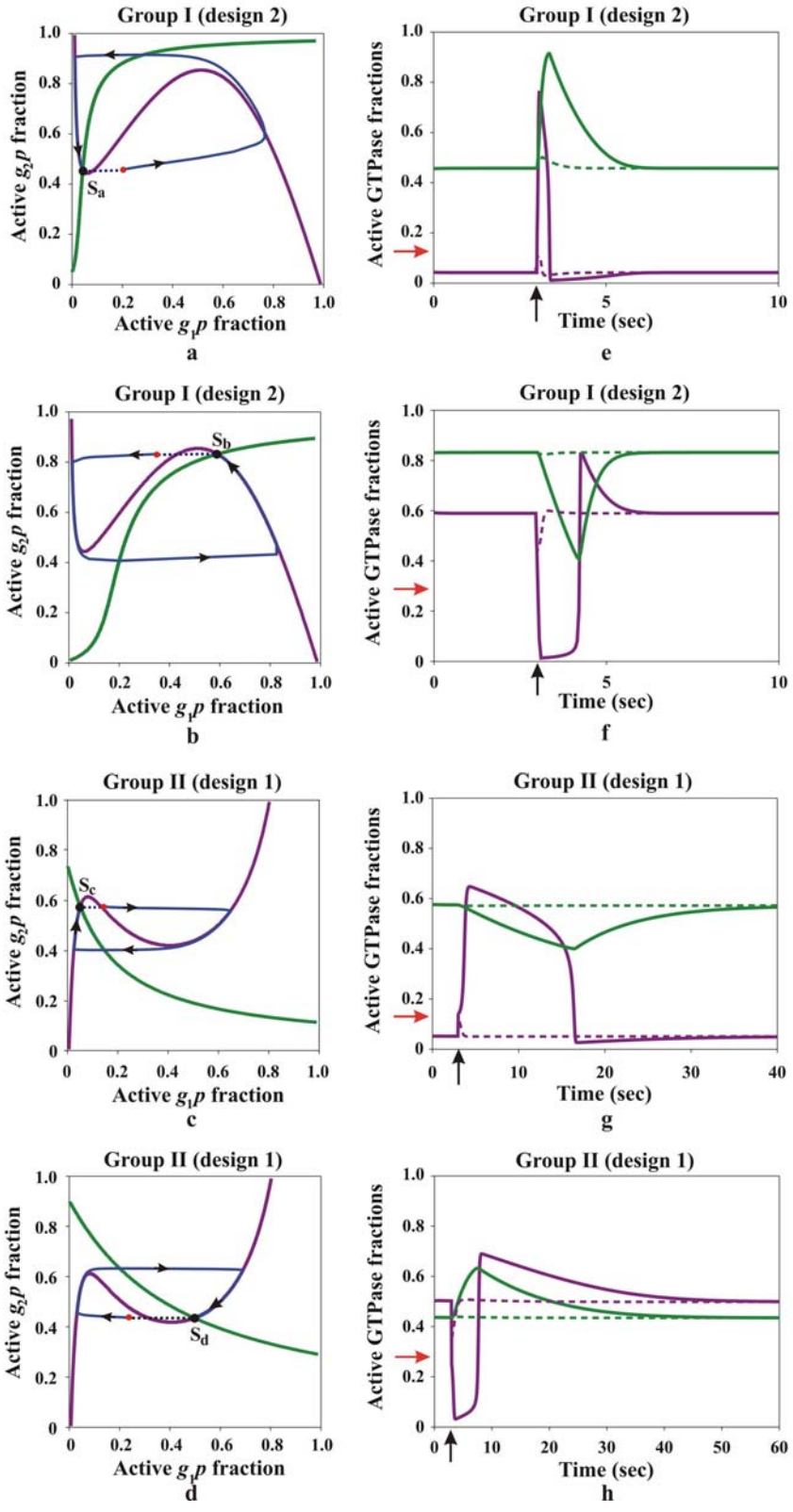

Fig. S4. Excitable behavior of GTPase cascades. Initially, each cascade resides in a stable, but excitable steady state. For group I cascades (**a, b**), the first g_1p-nullcline (purple) is N-mirror shaped, and the second g_2p-nullcline (green) is a monotone increasing function of g_1p. For group II cascades (**c, d**), the first g_1p-nullcline (purple) is N- shaped, and the second g_2p-nullcline (green) is a monotone

decreasing function of g_1p (**a - d**). The two nullclines intersect at a single point, corresponding to a stable steady state (S, bold black dot) positioned at the left arm (**a**, **c**) or the right arm (**b**, **d**) of the g_1p-nullcine. The different steady state positions are brought about by the changes in GEF_2 activity, described by the parameter r_3, whose magnitudes and the corresponding steady-state values of GTPase fractions (g_1p_{ss}, g_2p_{ss}) are given in Table S2. The trajectories (blue) presented on the phase plane (g_1p, g_2p) correspond to over-threshold perturbations (shown by dotted lines which start with steady-state values **S** and end with red dots). Panels (**e - h**) show temporal responses of active GTPase fractions, g_1p (purple) and g_2p (green), to sub-threshold (dashed lines) and over-threshold (solid lines) perturbations. At time t = 3 s (marked by black arrow), the steady-state concentration of the active GTPase at the first level (g_1p) is perturbed. Sub-threshold perturbations cause small responses shown by dashed lines. Over-threshold perturbations cause large overshoot responses where the active GTPase fractions can significantly increase or decrease, generating temporal pulses of GTPase activities (threshold values of g_1p perturbation amplitudes are marked by red arrows). It is instructive to note that while GEF_2 activity (r_3) varies (decreases for group I cascades or increases for group II cascades), the excitable regime, corresponding to the stable steady state positioned at the left arm of the g_1p-nullcline (**a**, **c**) becomes oscillatory, corresponding to the unstable steady state positioned at the middle arm (Fig. S3a). With a further change in r_3, the oscillatory regime becomes again excitable, corresponding to the stable steady state positioned at the left arm of the g_1p-nullcline (**b**, **d**).

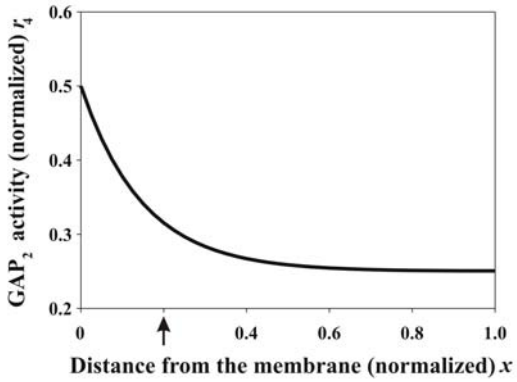

Fig. S5. Spatial gradient of GAP_2 constitutive activity. The activity (r_4) of GAP_2 decreases with the distance (x) from the plasma membrane, as specified by Eq. 10 in Methods. The kinetic parameter values are the following, $r_4(0)=0.5$, $r_4(1)=0.25$ (s^{-1}), and $\eta=6.7$. The arrow indicates the spatial coordinate where a transition from an oscillatory to excitable regime occurs (the Hopf bifurcation).

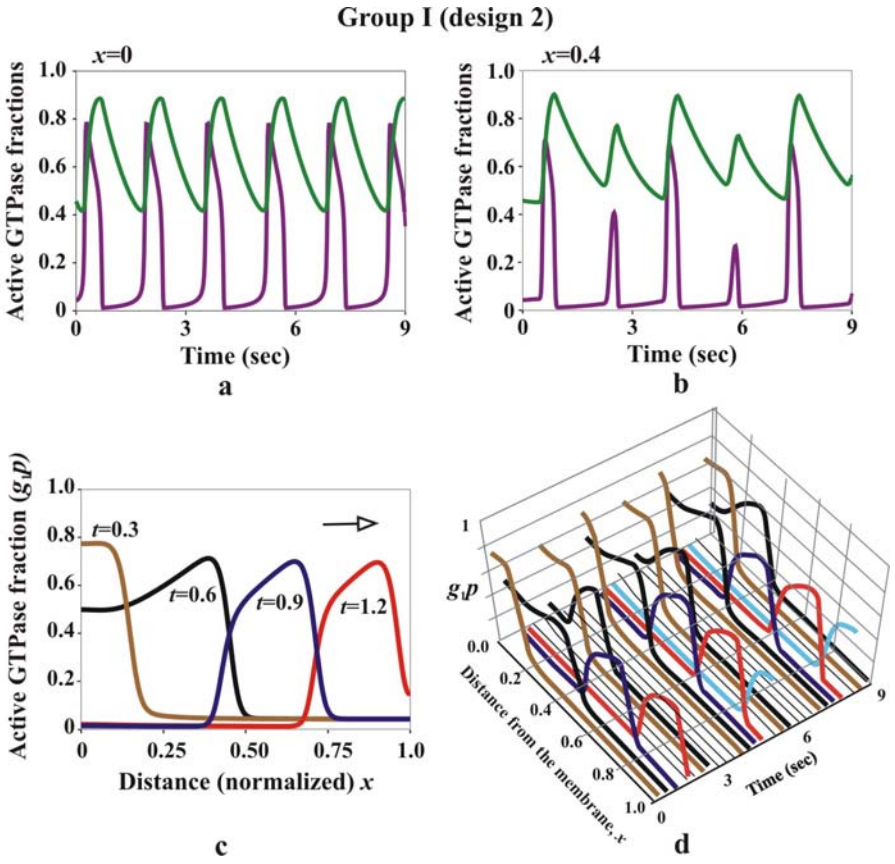

Fig. S6. Propagation or vanishing of periodic pulses in spatially heterogeneous media. The spatial gradient of GAP_2 constitutive activity is described by Eq. 10 (Methods) with slightly different kinetic parameters in comparison with Fig. 6, and Fig. S5: $r_4(0)=1$, $r_4(1)=0.5$, and $r_3= 0.4$ (s^{-1}). (**a**) Close to the membrane ($x \approx 0$), active GTPase fractions (g_1p, purple and g_2p, green) oscillate with a period of 1.5 s. A decrease in GAP_2 activity farther away from the membrane brings about the change in the cascade dynamics: oscillatory behavior is no longer observed, whereas excitable behavior emerges at $x \approx 0.2$ (the Hopf bifurcation). (**b**) Since this period of oscillations is smaller than the recovery time (known as the refractory period) of the emerging excitable media at the distance $x > 0.2$ from the membrane, not all oscillatory activity maxima lead to the formation of GTPase activity pulses with a large amplitude; some pulses become rather small and subsequently vanish during the propagation through the cell. (**c**) A pulse-like wave propagating through the cell is shown for a selected time window (0.3 - 1.2 s), using different colors for different time moments. (**c**) A 3-D presentation of propagating waves of periodic GTPase activity pulses driven by oscillating GTPase activities near the membrane. The remaining kinetic parameters and the initial GTPase activities, which correspond to a spatially homogeneous steady state, are given in Table S2.

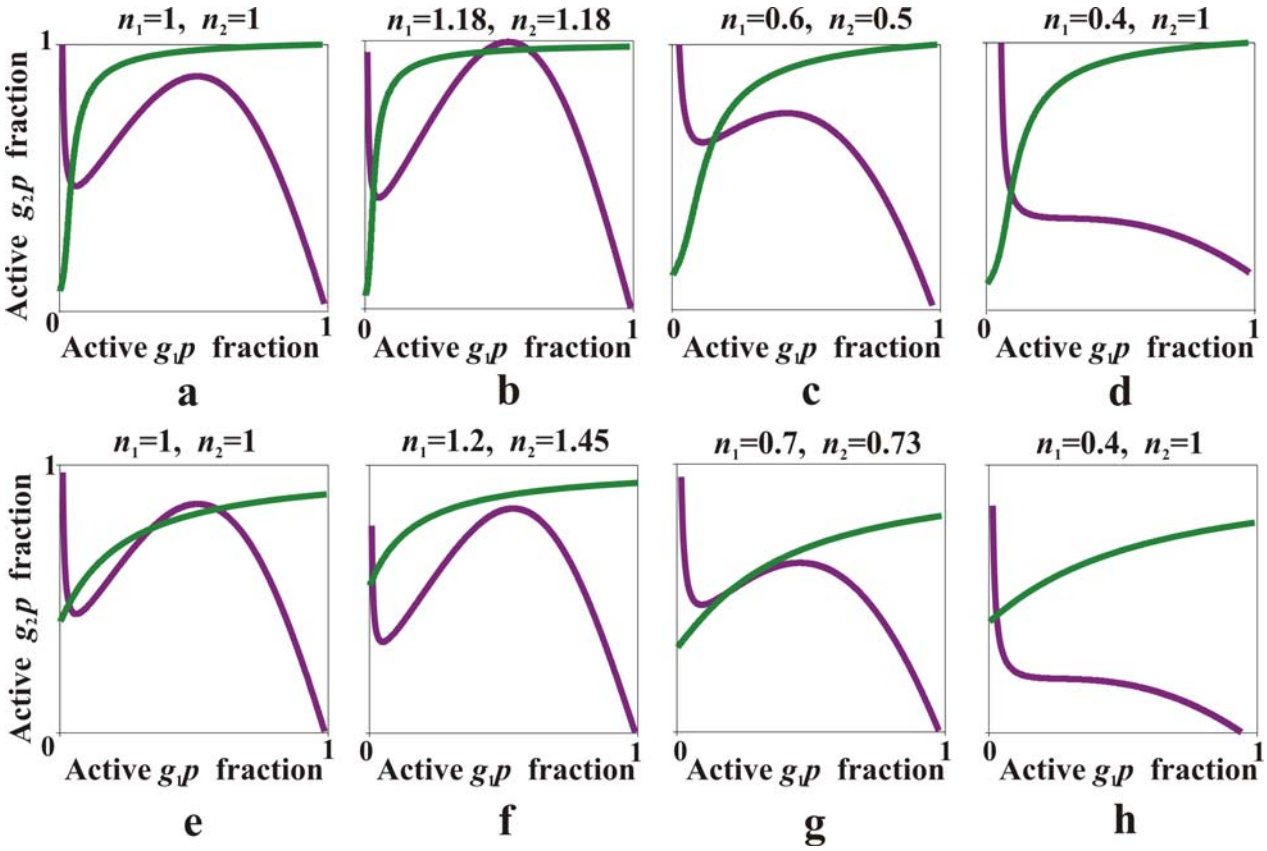

Fig. S7. Influence of the changes in the total GTPase abundances on the spatiotemporal cascade dynamics. The figure shows changes in the nullclines and the corresponding dynamic regimes following the alterations in the total abundance of the first and second GTPases (G_1^{tot} and G_2^{tot}), $G_{1new}^{tot} = n_1 \cdot G_1^{tot}$ and $G_{2new}^{tot} = n_2 \cdot G_2^{tot}$. According to Eqs. 1 -4 of the main text, this results in the following parameter changes: $m_1^{new} = m_1 / n_1$, $m_2^{new} = m_2 / n_1$, $m_3^{new} = m_3 / n_2$, $m_4^{new} = m_4 / n_2$, $m_{ij}^{new} = m_{ij} / n_i$. **a** -Excitable regime, the nullclines are calculated for parameter values given in Table S2. Following the changes in the total abundances as indicated by the coefficients n_1 and n_2, the system shifts to different dynamics regimes as follows, **b** - bistable, **c** - oscillatory, and **d** - monostable regimes. **e** -Bistable regime, the nullclines are calculated for parameter values given in Table S1. Following the changes in the total abundances as indicated by the coefficients n_1 and n_2, the system shifts to different dynamics regimes as follows, **f** -excitable, **g** - oscillatory, and **h** - monostable regimes.

Supplementary Documents.

Supplementary Document 1. Different design groups I - VIII are determined by the dimensionless multipliers α_{ij}.

Each cascade group I - VIII is characterized in by the values of the dimensional multipliers α_{ij}, as follows,

Groups I - IV are each hallmarked by an auto-activation loop, ($\alpha_{11} > 1$, $\alpha_{12} = 1$) or ($\alpha_{11} = 1$, $\alpha_{12} < 1$), and the remaining α_{ij} satisfy the following constraints,

Group I: ($\alpha_{21} < 1$, $\alpha_{22} = 1$) or ($\alpha_{21} = 1$, $\alpha_{22} > 1$); ($\alpha_{13} > 1$, $\alpha_{14} = 1$) or ($\alpha_{13} = 1$, $\alpha_{14} < 1$).

Group II: ($\alpha_{21} > 1$, $\alpha_{22} = 1$) or ($\alpha_{21} = 1$, $\alpha_{22} < 1$); ($\alpha_{13} < 1$, $\alpha_{14} = 1$) or ($\alpha_{13} = 1$, $\alpha_{14} > 1$).

Group III: ($\alpha_{21} > 1$, $\alpha_{22} = 1$) or ($\alpha_{21} = 1$, $\alpha_{22} < 1$); ($\alpha_{13} > 1$, $\alpha_{14} = 1$) or ($\alpha_{13} = 1$, $\alpha_{14} < 1$).

Group IV: ($\alpha_{21} < 1$, $\alpha_{22} = 1$) or ($\alpha_{21} = 1$, $\alpha_{22} > 1$); ($\alpha_{13} < 1$, $\alpha_{14} = 1$) or ($\alpha_{13} = 1$, $\alpha_{14} > 1$).

Groups V - VIII are each hallmarked by an auto-inhibition loop, ($\alpha_{11} < 1$, $\alpha_{12} = 1$) or ($\alpha_{11} = 1$, $\alpha_{12} > 1$), and the remaining α_{ij} satisfy the following constraints,

Group V: ($\alpha_{21} > 1$, $\alpha_{22} = 1$) or ($\alpha_{21} = 1$, $\alpha_{22} < 1$); ($\alpha_{13} > 1$, $\alpha_{14} = 1$) or ($\alpha_{13} = 1$, $\alpha_{14} < 1$).

Group VI: ($\alpha_{21} < 1$, $\alpha_{22} = 1$) or ($\alpha_{21} = 1$, $\alpha_{22} > 1$); ($\alpha_{13} < 1$, $\alpha_{14} = 1$) or ($\alpha_{13} = 1$, $\alpha_{14} > 1$).

Group VII: ($\alpha_{21} < 1$, $\alpha_{22} = 1$) or ($\alpha_{21} = 1$, $\alpha_{22} > 1$); ($\alpha_{13} > 1$, $\alpha_{14} = 1$) or ($\alpha_{13} = 1$, $\alpha_{14} < 1$).

Group VIII: ($\alpha_{21} > 1$, $\alpha_{22} = 1$) or ($\alpha_{21} = 1$, $\alpha_{22} < 1$); ($\alpha_{13} < 1$, $\alpha_{14} = 1$) or ($\alpha_{13} = 1$, $\alpha_{14} > 1$).

Supplementary Document 2. Relationships between kinetic parameters that enable identical steady states for molecular designs 1 - 8 comprising each topology group (I - VIII).

Using Table 1 (Methods), it is convenient to present the equations that determine nullclines for cascade designs 1 -8, as follows.

Definition of nullclines	Design 1	Design 2	Design 3	Design 4
$dg_1 p/dt = 0$ $dg_2 p/dt = 0$	$\alpha_{11}\alpha_{21}u_1 - u_2 = 0$ $\alpha_{13}u_3 - u_4 = 0$	$\alpha_{22}(\alpha_{11}\alpha_{22}^{-1}u_1 - u_2) = 0$ $\alpha_{13}u_3 - u_4 = 0$	$\alpha_{12}\alpha_{22}(\alpha_{12}^{-1}\alpha_{22}^{-1}u_1 - u_2) = 0$ $\alpha_{13}u_3 - u_4 = 0$	$\alpha_{12}(\alpha_{12}^{-1}\alpha_{21}u_1 - u_2) = 0$ $\alpha_{13}u_3 - u_4 = 0$
	Design 5	Design 6	Design 7	Design 8
$dg_1 p/dt = 0$ $dg_2 p/dt = 0$	$\alpha_{11}\alpha_{21}u_1 - u_2 = 0$ $\alpha_{14}(\alpha_{14}^{-1}u_3 - u_4) = 0$	$\alpha_{22}(\alpha_{11}\alpha_{22}^{-1}u_1 - u_2) = 0$ $\alpha_{14}(\alpha_{14}^{-1}u_3 - u_4) = 0$	$\alpha_{12}\alpha_{22}(\alpha_{12}^{-1}\alpha_{22}^{-1}u_1 - u_2) = 0$ $\alpha_{14}(\alpha_{14}^{-1}u_3 - u_4) = 0$	$\alpha_{12}(\alpha_{12}^{-1}\alpha_{21}u_1 - u_2) = 0$ $\alpha_{14}(\alpha_{14}^{-1}u_3 - u_4) = 0$

Comparing the nullcline equations of design 1 with such equations for designs 2 - 8 above, we can see that these nullclines become identical provided that the following relationships are satisfied:

Design 1 and Design 2:

$$\alpha_{11}^{(1)}\alpha_{21}^{(1)} = \alpha_{11}^{(2)}(\alpha_{22}^{(2)})^{-1} \Rightarrow \alpha_{11}^{(2)} = \alpha_{11}^{(1)},\ \alpha_{22}^{(2)} = 1/\alpha_{21}^{(1)} \Rightarrow \frac{1+a_{22}^{(2)}g_2 p/m_{22}^{(2)}}{1+g_2 p/m_{22}^{(2)}} = \frac{1+g_2 p/m_{21}^{(1)}}{1+a_{21}^{(1)}g_2 p/m_{21}^{(1)}} \Rightarrow$$

$$\Rightarrow (a_{22}^{(2)}a_{21}^{(1)}-1)g_2 p + (a_{22}^{(2)}m_{21}^{(1)} + a_{21}^{(1)}m_{22}^{(2)} - m_{21}^{(1)} - m_{22}^{(2)}) = 0 \Rightarrow a_{22}^{(2)}m_{21}^{(1)} + a_{21}^{(1)}m_{22}^{(2)} - m_{21}^{(1)} - m_{22}^{(2)} = 0 \Rightarrow$$

$$\Rightarrow m_{22}^{(2)}(a_{21}^{(1)}-1) = m_{21}^{(1)}(1-a_{22}^{(2)}) \Rightarrow \begin{cases} a_{22}^{(2)} = 1/a_{21}^{(1)} \\ m_{22}^{(2)} = m_{21}^{(1)}/a_{21}^{(1)} \end{cases}$$

Design 1 and Design 3:

$$\alpha_{11}^{(1)}\alpha_{21}^{(1)} = (\alpha_{12}^{(3)}\alpha_{22}^{(3)})^{-1} \Rightarrow \alpha_{12}^{(3)} = 1/\alpha_{11}^{(1)},\ \alpha_{22}^{(3)} = 1/\alpha_{21}^{(1)} \Rightarrow \begin{cases} a_{22}^{(3)} = 1/a_{21}^{(1)},\ m_{22}^{(3)} = m_{21}^{(1)}/a_{21}^{(1)} \\ a_{12}^{(3)} = 1/a_{11}^{(1)},\ m_{12}^{(3)} = m_{11}^{(1)}/a_{11}^{(1)} \end{cases}$$

Design 1 and Design 4:

$$\alpha_{11}^{(1)}\alpha_{21}^{(1)} = (\alpha_{12}^{(4)})^{-1}\alpha_{22}^{(4)} \Rightarrow \alpha_{22}^{(4)} = \alpha_{21}^{(1)},\ \alpha_{12}^{(4)} = 1/\alpha_{11}^{(1)} \Rightarrow a_{12}^{(4)} = 1/a_{11}^{(1)},\ m_{12}^{(4)} = m_{11}^{(1)}/a_{11}^{(1)}$$

Design 1 and Design 5:

$$\alpha_{11}^{(1)}\alpha_{21}^{(1)} = \alpha_{11}^{(5)}\alpha_{21}^{(5)} \Rightarrow \alpha_{11}^{(5)} = \alpha_{11}^{(1)},\ \alpha_{21}^{(5)} = \alpha_{21}^{(1)}$$

$$\alpha_{13}^{(1)} = (\alpha_{14}^{(5)})^{-1} \Rightarrow a_{14}^{(5)} = 1/a_{13}^{(1)},\ m_{14}^{(5)} = m_{13}^{(1)}/a_{13}^{(1)}$$

Design 1 and Design 6:

$$\begin{matrix} \alpha_{11}^{(1)}\alpha_{21}^{(1)} = \alpha_{11}^{(6)}(\alpha_{22}^{(6)})^{-1} \Rightarrow \alpha_{11}^{(6)} = \alpha_{11}^{(1)},\ \alpha_{22}^{(6)} = 1/\alpha_{21}^{(1)} \\ \alpha_{13}^{(1)} = (\alpha_{14}^{(6)})^{-1} \end{matrix} \Rightarrow \begin{cases} a_{22}^{(6)} = 1/a_{21}^{(1)},\ m_{22}^{(6)} = m_{21}^{(1)}/a_{21}^{(1)} \\ a_{14}^{(6)} = 1/a_{13}^{(1)},\ m_{14}^{(6)} = m_{13}^{(1)}/a_{13}^{(1)} \end{cases}$$

Design 1 and Design 7:

$$\begin{matrix} \alpha_{11}^{(1)}\alpha_{21}^{(1)} = (\alpha_{12}^{(7)}\alpha_{22}^{(7)})^{-1} \Rightarrow \alpha_{12}^{(7)} = 1/\alpha_{11}^{(1)},\ \alpha_{22}^{(7)} = 1/\alpha_{21}^{(1)} \\ \alpha_{13}^{(1)} = (\alpha_{14}^{(7)})^{-1} \end{matrix} \Rightarrow \begin{cases} a_{22}^{(7)} = 1/a_{21}^{(1)},\ m_{22}^{(7)} = m_{21}^{(1)}/a_{21}^{(1)} \\ a_{12}^{(7)} = 1/a_{11}^{(1)},\ m_{12}^{(7)} = m_{11}^{(1)}/a_{11}^{(1)} \\ a_{14}^{(7)} = 1/a_{13}^{(1)},\ m_{14}^{(7)} = m_{13}^{(1)}/a_{13}^{(1)} \end{cases}$$

Design 1 and Design 8:

$$\begin{matrix} \alpha_{11}^{(1)}\alpha_{21}^{(1)} = (\alpha_{12}^{(8)})^{-1}\alpha_{21}^{(8)} \Rightarrow \alpha_{12}^{(8)} = 1/\alpha_{11}^{(1)},\ \alpha_{21}^{(8)} = \alpha_{21}^{(1)} \\ \alpha_{13}^{(1)} = (\alpha_{14}^{(8)})^{-1} \end{matrix} \Rightarrow \begin{cases} a_{12}^{(8)} = 1/a_{11}^{(1)},\ m_{12}^{(8)} = m_{11}^{(1)}/a_{11}^{(1)} \\ a_{14}^{(8)} = 1/a_{13}^{(1)},\ m_{14}^{(8)} = m_{13}^{(1)}/a_{13}^{(1)} \end{cases}$$

The parameter relationships presented here in curly brackets are assembled in Table 1 (Methods).

Supplementary Document 3. Local stability and dynamic properties are identical for all 8 cascade circuitries within each of topology groups I - VIII.

We showed above that for the 8 different kinetic designs comprising each of groups I - VIII, the nullclines and steady states are identical if certain relationships between kinetic constants of regulatory interactions (feedback or feedforward loops) are fulfilled (Table 1, Methods and Supplementary material 2). Here we prove that the local stability and resulting dynamic properties of these designs are also the same. To simplify notations in the mathematical proofs, hereafter we designate the active GTPase fractions as follows,

$$y_1(t) = g_1 p(t),\ y_2(t) = g_2 p(t)\,.$$

It is convenient to introduce auxiliary parameters κ_1 and κ_2 as dimensionless multipliers, which modulate the rates (through modulation of constitutive GEF and GAP activities) at the first and second cascade layers, respectively. Thus, the parameter κ_1 is a dimensionless multiplier for the rates u_1 and u_2, and κ_2 is a multiplier of the rates u_3 and u_4. Using κ_1 and κ_2, the dynamics of cascade design 1 can be described as follows (see Eqs. 3, 4 in the main text and Table 1 in Methods),

$$\begin{aligned} \frac{dy_1}{dt} &= \kappa_1 \chi_1(y_1, y_2, p), \qquad \chi_1(y_1, y_2, p) = \alpha_{11}(y_1)\alpha_{21}(y_2)u_1(y_1) - u_2(y_1) \\ \frac{dy_2}{dt} &= \kappa_2 \chi_2(y_1, y_2, p), \qquad \chi_2(y_1, y_2, p) = \alpha_{13}(y_1)u_3(y_1, y_2) - u_4(y_2) \end{aligned} \qquad \text{(S1)},$$

where p is a vector of parameters, which include the kinetic constants and GEF and GAP concentrations (see Methods for the definitions of the functions α_{ij} and u_i).

If the relationships between kinetic parameters given in Table 1 (Methods) are fulfilled, the equations describing the dynamics of other designs 2 - 8, can be presented as,

$$\begin{aligned} \frac{dy_1}{dt} &= \varphi_1(y_1, y_2)\kappa_1 \chi_1(y_1, y_2, p) \\ \frac{dy_2}{dt} &= \varphi_2(y_1, y_2)\kappa_2 \chi_2(y_1, y_2, p) \end{aligned} \qquad \text{(S2)},$$

where the positive multipliers, $\varphi_i(y_1, y_2) > 0$, which determine a particular design are given in the table below,

	Designs							
	1	2	3	4	5	6	7	8
$\varphi_1(y_1, y_2) =$	1	$\alpha_{22}(y_2)$	$\alpha_{12}(y_1)\alpha_{22}(y_2)$	$\alpha_{12}(y_1)$	1	$\alpha_{22}(y_2)$	$\alpha_{12}(y_1)\alpha_{22}(y_2)$	$\alpha_2(y_1)$
$\varphi_2(y_1, y_2) =$	1	1	1	1	$\alpha_{14}(y_1)$	$\alpha_{14}(y_1)$	$\alpha_{14}(y_1)$	$\alpha_{14}(y_1)$

The steady states are determined as follows,

$$\frac{dy_1}{dt} = 0; \quad \frac{dy_2}{dt} = 0 \qquad \text{(S3)}.$$

One can readily see that the nullclines and steady states are identical for both systems 1 and 2 described by Eqs. S1 and S2, respectively. Let y_1^{ss}, y_2^{ss}, φ_1^{ss}, and φ_2^{ss} be the values of the variables y_1, y_2 and the functions φ_i at a particular steady state, where

$$\begin{aligned} &\chi_i(y_1^{ss}, y_2^{ss}, p) = 0 \\ &\varphi_i^{ss} = \varphi_i(y_1^{ss}, y_2^{ss}) > 0, \quad i = 1, 2 \end{aligned} \qquad \text{(S4)}.$$

We will next analyze the local stability (also termed exponential stability) of systems 1 and 2 near any steady state point. The Jacobian matrices ($\mathbf{J}_1$ and $\mathbf{J}_2$) for systems 1 and 2 at the steady state (y_1^{ss}, y_2^{ss}) are presented by Eqs. S5 and S6, respectively,

$$\mathbf{J}_1 = \begin{pmatrix} \kappa_1 \dfrac{\partial \chi_1}{\partial y_1} & \kappa_1 \dfrac{\partial \chi_1}{\partial y_2} \\ \kappa_2 \dfrac{\partial \chi_2}{\partial y_1} & \kappa_2 \dfrac{\partial \chi_2}{\partial y_2} \end{pmatrix}_{y_1^{ss}, y_2^{ss}} \tag{S5}.$$

$$\mathbf{J}_2 = \begin{pmatrix} \kappa_1 \left(\varphi_1 \dfrac{\partial \chi_1}{\partial y_1} + \chi_1 \dfrac{\partial \varphi_1}{\partial y_1} \right) & \kappa_1 \left(\varphi_1 \dfrac{\partial \chi_1}{\partial y_2} + \chi_1 \dfrac{\partial \varphi_1}{\partial y_2} \right) \\ \kappa_2 \left(\varphi_2 \dfrac{\partial \chi_2}{\partial y_1} + \chi_2 \dfrac{\partial \varphi_2}{\partial y_1} \right) & \kappa_2 \left(\varphi_2 \dfrac{\partial \chi_2}{\partial y_2} + \chi_2 \dfrac{\partial \varphi_2}{\partial y_2} \right) \end{pmatrix}_{y_1^{ss}, y_2^{ss}} = \begin{pmatrix} \varphi_1^{ss} \kappa_1 \dfrac{\partial \chi_1}{\partial y_1} & \varphi_1^{ss} \kappa_1 \dfrac{\partial \chi_1}{\partial y_2} \\ \varphi_2^{ss} \kappa_2 \dfrac{\partial \chi_2}{\partial y_1} & \varphi_2^{ss} \kappa_2 \dfrac{\partial \chi_2}{\partial y_2} \end{pmatrix}_{y_1^{ss}, y_2^{ss}} \tag{S6}.$$

We see that for system 2, the determinant of the Jacobian matrix $\mathbf{J}_2$ is multiplied by a positive factor that equals the product of φ_1^{ss} and φ_2^{ss}. Therefore, the condition det($\mathbf{J}$) = 0 will be true (or false) at the same parameter values for both systems 1 and 2. Consequently, if the saddle-node bifurcation occurs, it will take place for both systems simultaneously. However, Eq. S6 shows that the trace of the Jacobian is different for these two systems,

$$\mathrm{tr}(\mathbf{J}_1) = \kappa_1 \frac{\partial \chi_1}{\partial y_1} + \kappa_2 \frac{\partial \chi_2}{\partial y_2} \tag{S7}$$

and

$$\mathrm{tr}(\mathbf{J}_2) = \varphi_1^{ss} \kappa_1 \frac{\partial \chi_1}{\partial y_1} + \varphi_2^{ss} \kappa_2 \frac{\partial \chi_2}{\partial y_2} \tag{S8}.$$

Therefore, at first glance, the eigen values of the Jacobians $\mathbf{J}_1$ and $\mathbf{J}_2$ are not equal. Can we still say something about the local stability of a steady state of system 2, if we know the local stability of the same steady state of system 1?

Fortunately, the dimensionless multipliers, κ_1 and κ_2, can be modified without any change of the steady state values, y_1^{ss}, y_2^{ss}. If for system 2, we select the κ_1^* and κ_2^* values, as follows, $\varphi_1^{ss} \kappa_1^* = \kappa_1$, $\varphi_2^{ss} \kappa_2^* = \kappa_2$, then the Jacobians of both systems 1 and 2 become identical at the same steady state, y_1^{ss}, y_2^{ss},

$$\mathbf{J}_1(\kappa_1, \kappa_2) = \mathbf{J}_2(\kappa_1^*, \kappa_2^*).$$

This proves that both systems 1 and 2 (which are described by Eq. S1 and S2, respectively) can have the same Jacobian eigen values for the stationary solution, and thus possess similar local stability and dynamic properties (although at different parameter values, at the value κ_1 and κ_2 for system 1 and κ_1^* and κ_2^* for system S2).

Supplementary Document 4. Nullcline analysis.

First we show that for topology groups I - VIII, the g_2p-nullcline is a monotone function of g_1p for kinetic parameter values. Since for all 8 cascade designs within each topology group, the nullclines are identical when the proper relationships between the regulatory loop constants are fulfilled (see Table 1, Methods), we only consider nullclines for kinetic design 1.

As above, we simplify notations by designating $y_1(t) = g_1 p(t)$, $y_2 = g_2 p(t)$. For cascade design 1 in each topology group (I - VIII), the g_2p-nullcline ($dy_2/dt = 0$) is determined as follows (see Eqs. 3 and 4 and Table 1, Methods),

$$r_3 \cdot \frac{1 + a_{13} y_1 / m_{13}}{1 + y_1 / m_{13}} \cdot \frac{(1 - y_2)/m_3}{1 + (1 - y_2)/m_3} - r_4 \cdot \frac{y_2 / m_4}{1 + y_2 / m_4} = 0 \qquad \text{(S9)}.$$

Rearranging, we obtain,

$$(a_{13} - Y(y_2)) y_1 = m_{13}(Y(y_2) - 1) \qquad \text{(S10)}.$$

Here the function Y is introduced to simplify notations,

$$Y(y_2) = \frac{r_4 y_2 (m_3 + 1 - y_2)}{r_3 (m_4 + y_2)(1 - y_2)} \qquad \text{(S11)}.$$

We will show now that $a_{13} \neq Y$ for any y_2 value, $0 < y_2 < 1$. Assuming that $a_{13} - Y(y_2) = 0$ for some y_2, it follows that the right hand side of Eq. S10 should equal 0, that is, $Y(y_2) = 1$. Then from our initial assumption, a_{13} must be equal to 1. Recall that for design 1 in each topology group, $a_{13} \neq 1$, and so our assumption that $a_{13} - Y(y_2) = 0$ must be false, and this proves that $a_{13} \neq Y$.

Using Eq. S10, y_1 can be presented as the following function of y_2,

$$y_1(y_2) = m_{13} \frac{Y(y_2) - 1}{a_{13} - Y(y_2)} \qquad \text{(S12)}.$$

If the function $y_1(y_2)$ is not monotone, then the derivative dy_1 / dy_2 must equal zero at some y_2,

$$\frac{dy_1}{dy_2} = \frac{m_{13}(a_{13} - 1)}{(a_{13} - Y(y_2))^2} Y'(y_2) = 0 \qquad \text{(S13)}.$$

This implies that $dY / dy_2 = 0$ at some y_2. Differentiating Eq. S11 results in the following quadratic equation for the y_2 value(s), at which Eq. S13 holds,

$$(m_3 + m_4) y_2^2 - 2 m_4 y_2 + (m_3 + 1) m_4 = 0 \qquad \text{(S14)}.$$

Since the discriminant of this quadratic equation is negative,

$D = 4m_4^2 - 4(m_3 + 1) m_4 (m_3 + m_4) = -4m_3 (m_4^2 + (m_3 + 1) m_4) < 0$,

Eq. S13 does not have real value solutions. This proves that the g_2p-nullcline, $dy_2/dt = 0$, is a monotone function. From Eq. S13, we can see that the sign of the derivative, dy_2/dy_1 is determined by the

difference, $a_{13}-1$. If $a_{13}>1$, the g_2p-nullcline is a monotone increasing function of g_1p, and when $a_{13}<1$, the g_2p-nullcline is a monotone decreasing function. This proves that for cascade designs comprising groups I, III, V and VII, the g_2p-nullcline is a monotone increasing function, and this nullcline is a monotone decreasing function for cascades in groups II, IV, VI, VIII (see Fig. 3 and Fig. S2, S3 and S4).

Next we show that for topology groups V - VIII, the g_1p-nullcline is a monotone function of g_2p for any values of kinetic parameters. As above, it is sufficient to consider only kinetic design 1. The g_1p-nullcline for cascade design 1 can be determined from the following equation, $dy_1/dt = 0$,

$$r_1\frac{1+a_{11}\cdot y_1/m_{11}}{1+y_1/m_{11}}\frac{1+a_{21}\cdot y_2/m_{21}}{1+y_2/m_{21}}\frac{(1-y_1)/m_1}{1+(1-y_1)/m_1}-r_2\frac{y_1/m_2}{1+y_1/m_2}=0 \qquad \text{(S15).}$$

Rearranging, we obtain,

$$(a_{21}-Z(y_1))y_2(y_1)=m_{21}(Z(y_1)-1) \qquad \text{(S16).}$$

Here $$Z(y_1)=\frac{r_2y_1(m_1+1-y_1)(y_1+m_{11})}{r_1(m_2+y_1)(m_{11}+a_{11}y_1)(1-y_1)} \qquad \text{(S17).}$$

Since for design 1 in each topology group, $a_{21}\neq 1$, it can be shown that $a_{21}\neq Z$ for any for any y_1 value, $0<y_1<1$. Similar to above, the assumption $a_{21}-Z=0$ for some y_2 would imply that a_{21} must be equal 1, which is untrue for design 1. From Eq. (S16), it follows that,

$$y_2(y_1)=m_{21}\frac{Z(y_1)-1}{a_{21}-Z(y_1)} \qquad \text{(S18).}$$

If the function $y_2(y_1)$ is not monotone, then the derivative dy_2/dy_1 must equal zero at some y_1,

$$\frac{dy_2}{dy_1}=\frac{m_{21}(a_{21}-1)}{(a_{21}-Z(y_1))^2}Z'(y_1)=0 \qquad \text{(S19).}$$

Differentiating the function Z, we obtain the following equation for the y_1 value that satisfies Eq. (S19),

$$c_4y_1^4+c_3y_1^3+c_2y_1^2+c_1y_1+c_0=0 \qquad \text{(S20),}$$

where the parameter values are given as follows,

$$\begin{aligned}
c_4&=m_{11}(1-a_{11})+a_{11}m_1+a_{11}m_2\\
c_3&=2(a_{11}m_{11}(m_1+1)+m_{11}m_2-m_{11}-a_{11}m_2)\\
c_2&=m_{11}{}^2m_2+m_{11}{}^2m_1+a_{11}m_{11}km_1+m_{11}(m_1+1)(1-a_{11})+a_{11}m_2(m_1+1)-m_{11}m_2(m_1+1)-3m_{11}m_2\\
c_1&=2(m_{11}m_2(m_1+1)-m_{11}{}^2m_2)\\
c_0&=m_{11}{}^2m_2(m_1+1)
\end{aligned} \qquad \text{(S21).}$$

Taking Eq. S21 into consideration, it is convenient to regroup the different terms of Eq. S20, presenting this equation as the sum of the five following terms,

$$\mu_1+\mu_2+\mu_3+\mu_4+\mu_5=0 \qquad \text{(S22),}$$

where,

$$\mu_1 = a_{11} m_1 y_1^4 + [m_{11}{}^2 m_1 + a_{11} m_{11} m_2 m_1] y_1^2$$
$$\mu_2 = m_{11}(1-a_{11}) y_1^4 - 2m_{11}(1-a_{11}(m_1+1) y_1^3 + m_{11}(m_1+1)(1-a_{11}) y_1^2 > m_{11} y_1^2 (1-a_{11})[y_1^2 - 2y_1 + (m_1+1)]$$
$$\mu_3 = a_{11} m_2 y_1^4 - 2a_{11} m_2 y_1^3 + a_{11} m_2 (m_1+1) y_1^2 = a_{11} m_2 y_1^2 (y_1^2 - 2y \ + (m_1+1)) = a_{11} m_2 y_1^2 [(y_1-1)^2 + m_1]$$
$$\mu_4 = m_{11}^2 m_2 y_1^2 - 2m_{11}^2 m_2 y_1 + m_{11}^2 m_2 (m_1+1) = m_{11}^2 m_2 (y_1^2 - 2y_1 + (m_1+1)) = m_{11}^2 m_2 [(y_1-1)^2 + m_1]$$
$$\mu_5 = 2m_{11} m_2 y_1^3 - (3m_{11} m_2 + m_{11} m_2 (m_1+1)) y_1^2 + 2m_{11} m_2 (m_1+1) y_1 = m_{11} m_2 y_1 [2y_1^2 - (4+m_1) y_1 + 2(m_1+1)] =$$
$$= 2(1-y_1)^2 + 2m_1 (1-y_1) + m_1 y_1$$

Since all kinetic constants are positive and $a_{11} < 1$ for each group V-VIII (hallmarked by an auto-inhibitory loop, Fig. 1b), one can readily see that each term (μ_1, μ_2, μ_3, μ_4, μ_5) is positive, and therefore the left-hand side of Eq. S20 is always positive. This proves that for cascade designs comprising groups V-VIII, Eq. S19 does not have solutions for any $0 < y_1 < 1$, and the g_1p-nullcline, $dy_1/dt = 0$, is monotone function. The sign of the derivative, dy_1/dy_2 is determined by the sign of the difference, $a_{21} - 1$ (see Eq. S13). If $a_{21} > 1$, the g_1p-nullcline is monotone increasing function, and when $a_{21} < 1$, the g_1p-nullcline is monotone decreasing function. This proves that for cascade designs in groups V and VIII, the g_1p-nullcline is a monotone increasing function, whereas for groups VI and VII the g_1p-nullcline is a monotone decreasing function (see Fig. 3 and Fig.S2).

Supplementary Document 5. Influence of small G-protein overexpression on the spatiotemporal cascade dynamics.

Many GTPases are overexpressed in cancer [1]. Although increases in the total GTPase abundances (G_1^{tot} and G_2^{tot}) can change the spatiotemporal dynamics, a particular G-protein cascade still belongs to the same topology group. In fact, different topology groups are determined by the dimensionless multipliers a_{ij} that do not depend on G_1^{tot} and G_2^{tot} (see Materials and Methods, Eqs 2 and 4, and Supplementary Document 1). Therefore, merely overexpression of small G-proteins, but not a mutation that can make it constantly active, does not change the types of possible dynamic behaviors in time and space. Moreover, under specific saturating conditions the basal GTPase fractions at steady state are relatively insensitive to GTPase overexpression [1]. Yet in the other cellular context, even relatively small variations in the total GTPase abundances can dramatically change the cascade dynamic behavior, as illustrated in Fig. S7.

References.

1. S. Legewie, C. Sers and H. Herzel, *FEBS Lett*, 2009, **583**, 93-96.

Table S1. Kinetic parameters of bistable regimes and active GTPase fractions (g_1p_{ss} and g_2p_{ss}) at two different steady states S_1 and S_2 for cascade design 1 in groups I – VI[*].

	Design 1											
	Group I		**Group II**		**Group III**		**Group IV**		**Group V**		**Group VI**	
r_1 (s^{-1})	5		10		1		1		1		1	
r_2 (s^{-1})	4		6.5		0.65		0.8		1.6		0.13	
r_3 (s^{-1})	0.13		0.4		0.5		0.1		1		1	
r_4 (s^{-1})	0.072		0.7		0.6		0.5		3		0.01	
m_1	0.7		25		25		0.7		1		0.4	
m_2	0.15		0.09		0.09		0.15		5		0.09	
m_3	0.6		5		5		0.8		2		0.1	
m_4	0.05		14		5.5		8		0.005		0.05	
a_{11}	200		200		200		200		0.01		0.6	
m_{11}	4		10		10		4		0.005		0.1	
a_{13}	100		0.005		40		0.05		100		0.004	
m_{13}	40		0.5		10		0.3		3		0.002	
a_{21}	0.02		80		80		0.02		100		0.01	
m_{21}	0.04		20		20		0.04		2		0.1	
	Steady states		Steady states		Steady states		Steady states		Steady states		Steady states	
	S_1	S_2	S_1	S_2	S_1	S_2	S_1	S_2	S_1	S_2	S_1	S_2
g_1p_{ss}	0.035	0.59	0.055	0.485	0.038	0.756	0.023	0.91	0.1	0.483	0.078	0.83
g_2p_{ss}	0.48	0.83	0.586	0.43	0.516	0.8	0.56	0.23	0.0045	0.49	0.94	0.68

[*]The input GEF_1 activity (parameter r_1) is varied to obtain the hysteretic plots shown in Fig. 3 (right panels) of the main text. In Figs. 5 and 6 of the main text the relationships between the kinetic parameters of designs 1 and 2 is given in Table I (Methods).

Table S2. Kinetic parameters of oscillatory and excitable regimes and active GTPase fractions (g_1p_{ss} and g_2p_{ss}) at steady states for cascade design 1 in groups I and II.

	Design 1					
	Group I			**Group II**		
	Oscillatory	**Excitable**		**Oscillatory**	**Excitable**	
$r_1(s^{-1})$	5	5		10	10	
$r_2(s^{-1})$	4	4		6.5	6.5	
$r_3(s^{-1})$	0.2	0.4*, 0.125*		1	0.55**, 1.7**	
$r_4(s^{-1})$	0.5	0.5		0.55	0.55	
m_1	0.7	0.7		25	25	
m_2	0.15	0.15		0.09	0.09	
m_3	0.6	0.6		5	5	
m_4	0.05	0.05		14	14	
a_{11}	200	200		200	200	
m_{11}	4	4		10	10	
a_{13}	100	100		0.005	0.005	
m_{13}	3	3		0.05	0.05	
a_{21}	0.02	0.02		80	80	
m_{21}	0.04	0.04		20	20	
	-----	Steady states		-----	Steady states	
		S_a	S_b		S_c	S_d
g_1p_{ss}	-----	0.044	0.59	-----	0.05	0.5
g_2p_{ss}		0.46	0.83		0.58	0.44

*Group I: r_3= 0.4 and steady state S_a correspond to Figs.4e, 5c and 6 of the main text and Fig.S4a; r_3= 0.125 and steady state S_b correspond to Figs. 4f and 5d of the main text and Fig.S4b.

**Group II: r_3= 0.55 and steady state S_c correspond to Fig. 4g of the main text and Fig.S4c; r_3= 1.7 and steady state S_d correspond to Fig. 4h of the main text and Fig.S4d.

For Fig. 4-6 of the main text the relationships between the kinetic parameters of designs 1, 2 and 5 are given in Table I (Methods).

Table S3. Kinetic parameters of bistable, oscillatory and excitable regimes and active GTPase fractions (g_1p_{ss} , g_2p_{ss} and g_3p_{ss}) at two different steady states S_1 and S_2 of a 3-tier cascade shown in Fig. 7 in the main text*

	Bistable		Oscillatory	Excitable
$r_1(s^{-1})$	1		1	8
$r_2(s^{-1})$	20		35	80
$r_3(s^{-1})$	5		50	50
$r_4(s^{-1})$	4		40	40
$r_5(s^{-1})$	0.12		0.12	0.12
$r_6(s^{-1})$	0.75		0.75	0.75
m_1	0.5		1.45	1.45
m_2	0.005		1.2	0.01
m_3	0.7		0.7	0.7
m_4	0.15		0.15	0.15
m_5	0.6		0.6	0.6
m_6	0.05		0.05	0.05
a_{13}	100		100	100
m_{13}	2		2	2
a_{21}	200		200	200
m_{21}	4		4	4
a_{25}	100		100	100
m_{25}	15		3	3
a_{34}	50		50	50
m_{34}	2		2	2
	Steady states		-	Steady state
	S_1	S_2		S
g_1p_{ss}	0.0025	0.456		0.003
g_2p_{ss}	0.19	0.91		0.11
g_3p_{ss}	0.014	0.09		0.04

*The steady-state values of active GTPase fractions (g_1p_{ss}, g_2p_{ss}, g_3p_{ss}) were used as the initial spatially homogeneous conditions in Fig. 7c (steady state S_1) and Fig. 7d (steady state S) of the main text. The initial perturbation in Fig. 7c was the following, $g_1p(x,0) = 0.8$ for $0 \le x \le 0.03$.

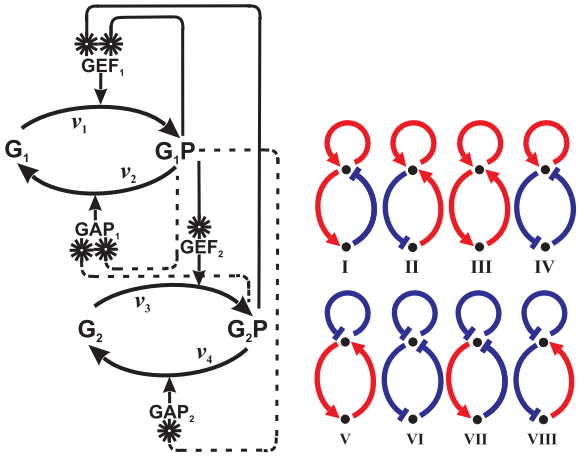

a b

Fig1 eps

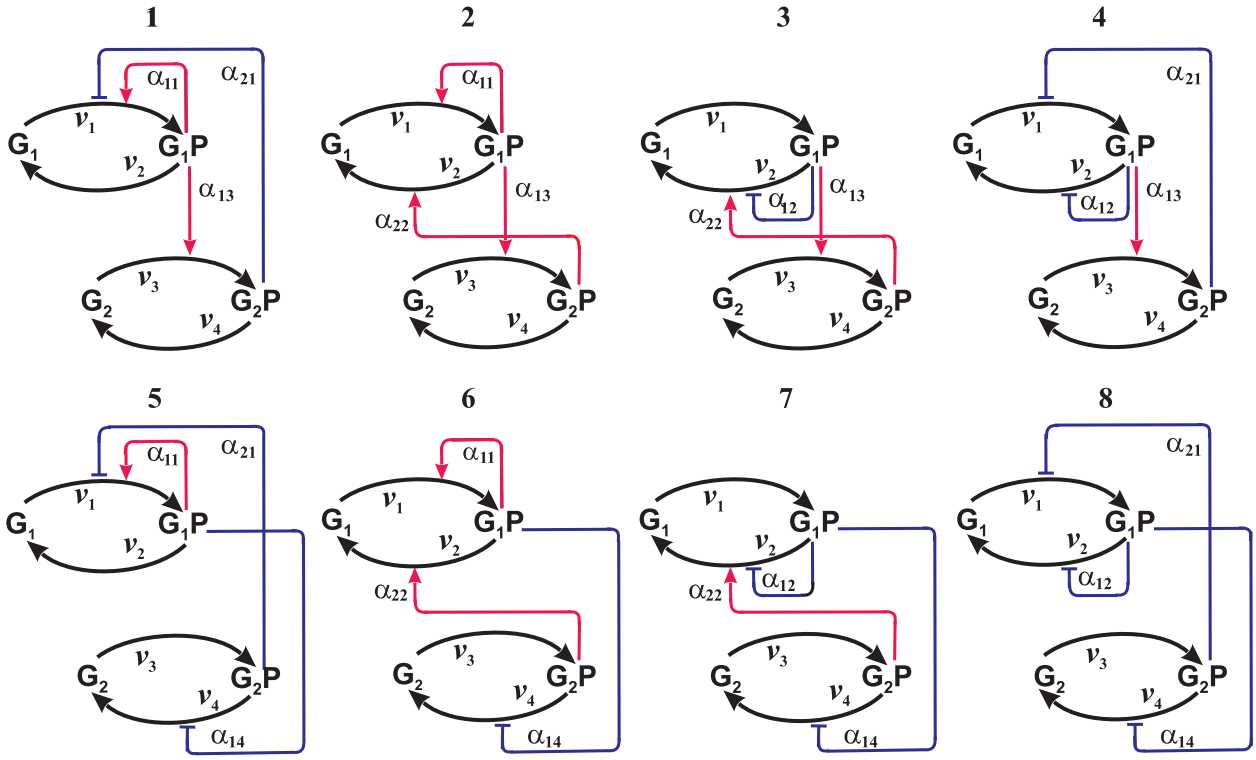

Fig2.eps

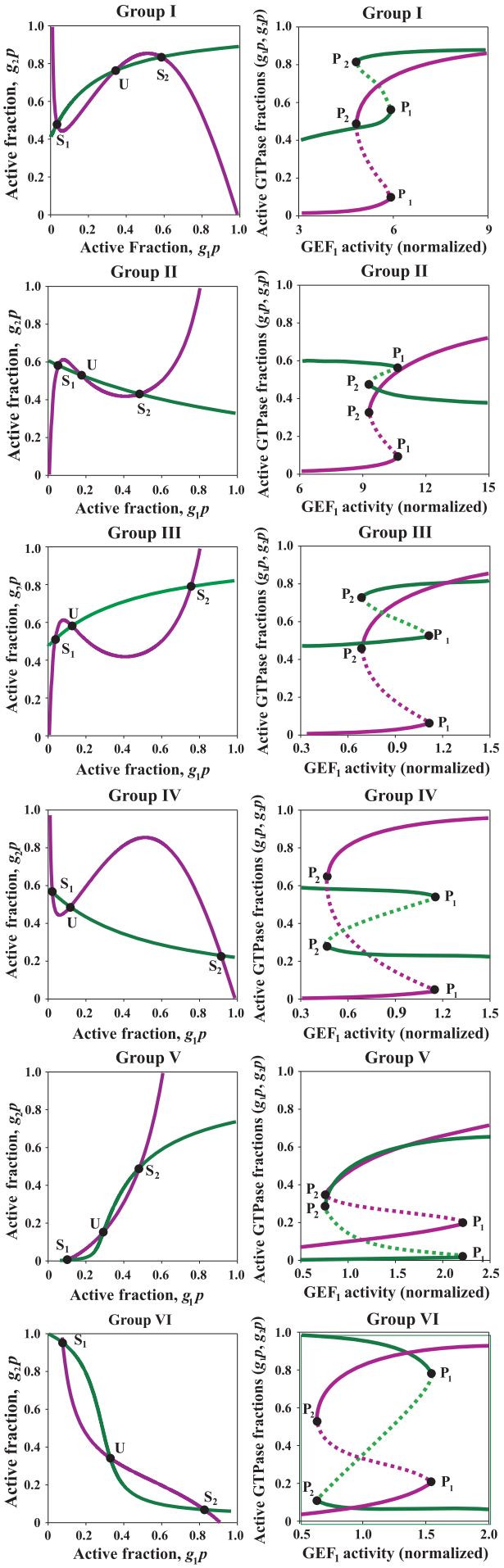
Group I
Active fraction, g_2p
Active Fraction, g_1p
U
S_1
S_2
Active GTPase fractions (g_1p, g_2p)
GEF_1 activity (normalized)
P_2
P_1
Group II
Group III
Group IV
Group V
Group VI

Fig3.eps

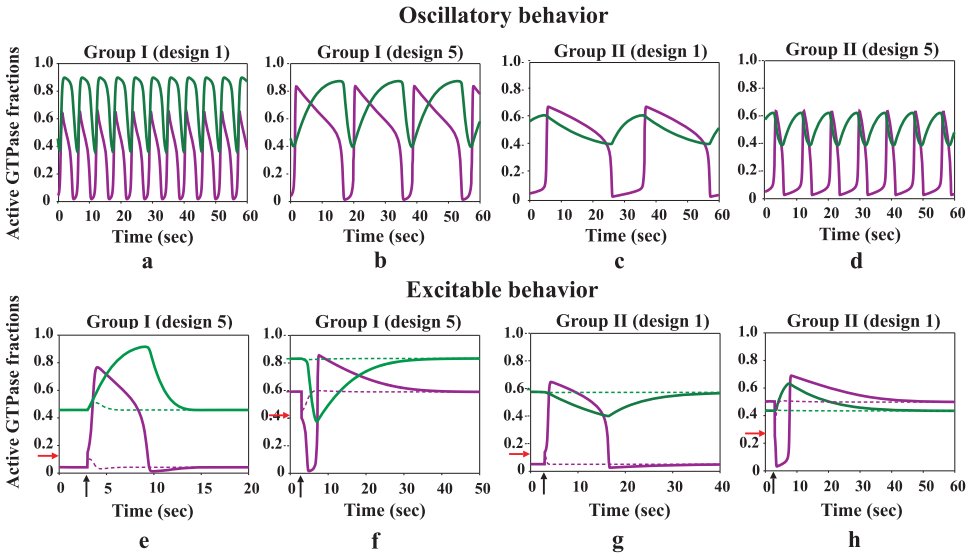

Fig4.eps

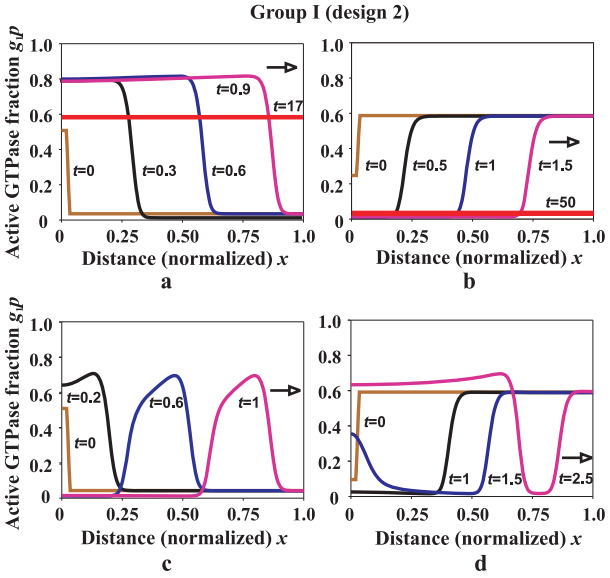

Figs5.eps

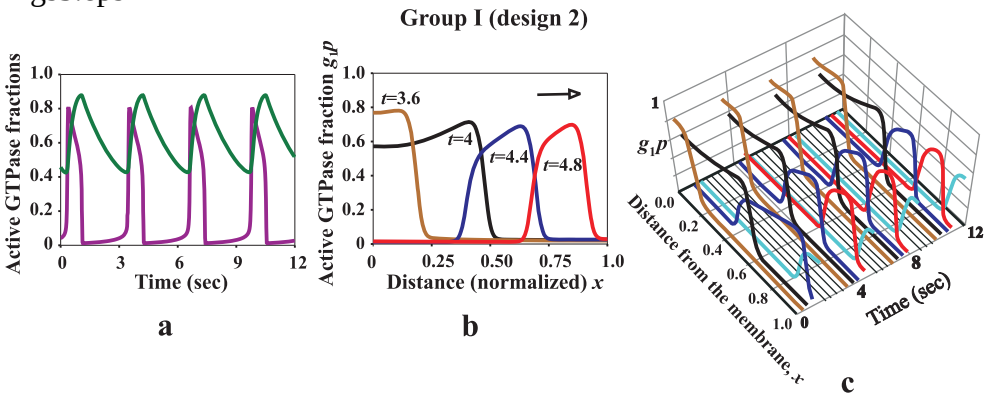

Fig6.eps

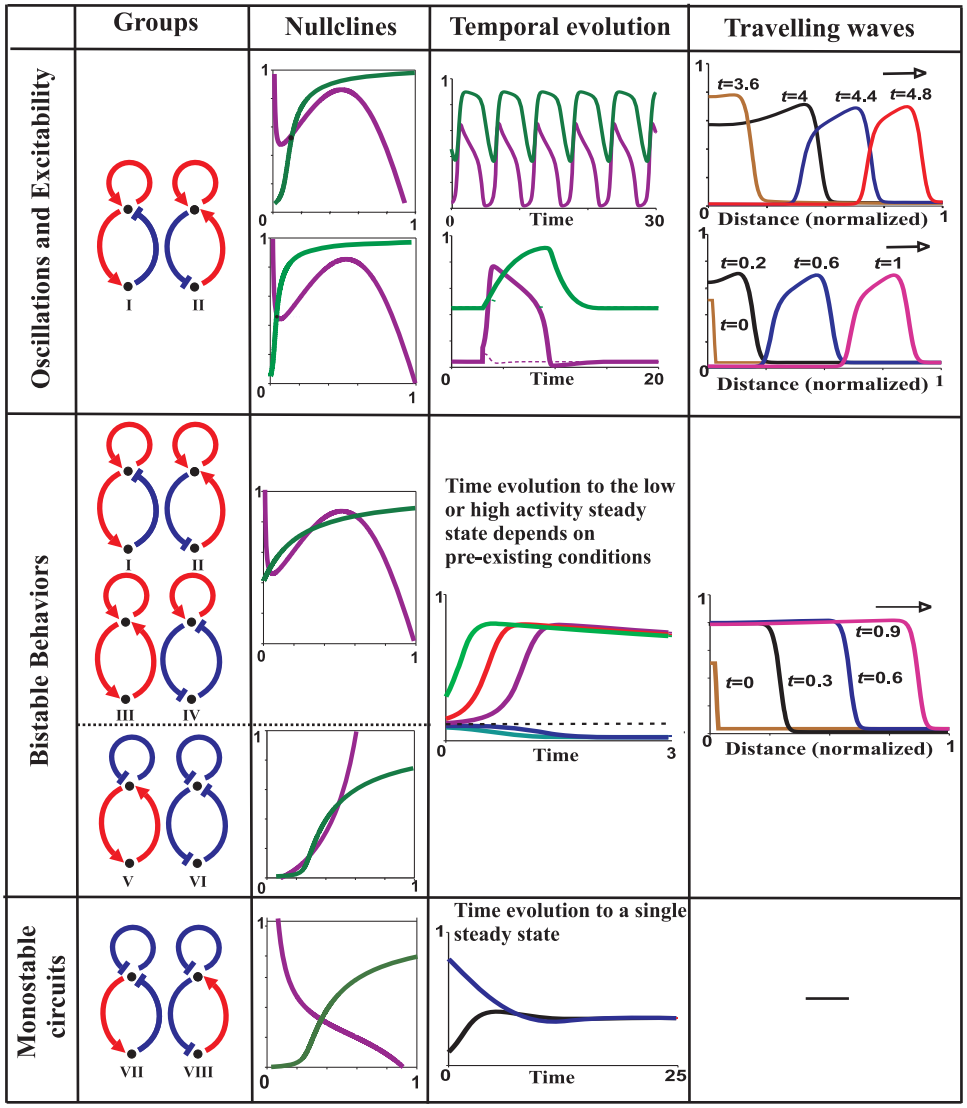

Fig7.eps

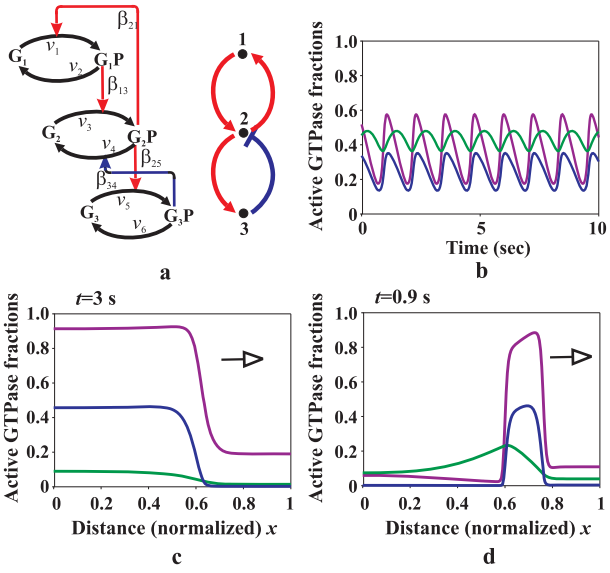

Fig8.eps